Please cite this article in press as: Abdel-Latif et al., Flow Synthesis of Metal Halide Perovskite Quantum Dots: From Rapid Parameter Space Mapping to AI-Guided Modular Manufacturing, Matter (2020), https://doi.org/10.1016/j.matt.2020.07.024

Matter

CellPress

Review

Flow Synthesis of Metal Halide Perovskite Quantum Dots: From Rapid Parameter Space Mapping to AI-Guided Modular Manufacturing

Q1 Kameel Abdel-Latif,[1,2] Fazel Bateni,[1,2] Steven Crouse,[1] and Milad Abolhasani[1,*]

SUMMARY

Microscale flow synthesis is a versatile technology for accelerated materials development and rapid process-structure-property mapping of solution-processed materials. Lead (Pb) halide perovskite quantum dots (PQDs), with their outstanding optoelectronic properties and widespread applications in photonic devices, are an exciting high-priority material candidate for rapid exploration with flow synthesis strategies. Modular and reconfigurable flow synthesis platforms equipped with precursor formulation, controlled flow synthesis, and *in situ* diagnostic modules can enable high-throughput experimentation with real-time access to Pb halide PQD optoelectronic properties. In this review, we discuss recent efforts focused on *in situ* characterization, post-processing, artificial intelligence (AI)-enhanced synthesis optimization, and mechanistic studies of Pb halide PQDs conducted utilizing flow synthesis techniques. Furthermore, we provide an overview of the recently developed AI-guided flow synthesis strategies for accelerated development and continuous manufacturing of Pb halide PQDs. Finally, we present current challenges and potential future directions toward enabling end-to-end continuous manufacturing of application-ready PQDs.

Progress and Potential

Over the past 5 years, lead halide perovskite quantum dots (PQDs) have received significant attention due to their unique size-, composition-, and process-dependent optoelectronic properties, as well as their applications in energy and chemical technologies. However, the development pace of this remarkable class of semiconductor nanocrystals is hindered mainly because of the inherent limitations imposed by commonly employed batch synthesis methods. Recent advancements of flow synthesis strategies integrated with *in situ* material diagnostic probes have proved their potential to outperform the conventional batch synthesis tools toward accelerated development, optimization, and continuous manufacturing of lead halide PQDs. Furthermore, the prospect of autonomous materials development in flow through convergence of modular flow synthesis platforms with rapidly emerging artificial intelligence-guided decision-making strategies provides a unique opportunity for further acceleration of research and development in the field of metal halide PQDs.

Q3 Q2 INTRODUCTION

Since their discovery in 2015,[1] lead (Pb) halide perovskite quantum dots (PQDs) have gained significant attention for a wide range of applications in energy and chemical technologies, including photovoltaics,[2–7] light-emitting diodes (LEDs),[8–10] displays,[11] lasers,[12] photocatalysis,[13–15] and photodetectors.[16] As a new class of quantum dots (QDs), Pb halide PQDs have exhibited outstanding performance in the field owing to their unique size- and composition-dependent optoelectronic properties, including narrow photoluminescence (PL) bandwidth, high mobility and long diffusion path length of charge carriers, and near-unity PL quantum yield (PLQY > 95%).[1,17–21]

The relatively high PLQY and optical absorption of Pb halide PQDs are mainly attributed to their defect-tolerant crystalline structure combined with high mobility of charge carriers, which diminish the possibility of non-radiative exciton recombination.[1,22–26] Pb halide PQDs can be broadly categorized into two groups of fully inorganic and hybrid organic-inorganic PQDs with the common formula of $APbX_3$, in which A represents monovalent organic/inorganic cations (e.g., cesium [Cs], formamidinium [FA], methylammonium [MA], or a mixture of cations), and X represents halide anions (Cl^-, Br^-, I^-, or mixed halides). In their three-dimensional perovskite structure, Pb and halide ions form a network of corner-shared octahedra, [PbX_6],

Please cite this article in press as: Abdel-Latif et al., Flow Synthesis of Metal Halide Perovskite Quantum Dots: From Rapid Parameter Space Mapping to AI-Guided Modular Manufacturing, Matter (2020), https://doi.org/10.1016/j.matt.2020.07.024

in which the voids created by the [PbX_6] network are filled with A-site cations (Figure 1).[27,28] Moreover, to maintain the stability and symmetry of the perovskite structures, the choice of A-site cations (or mixed cations) must meet the size restrictions determined by the Goldschmidt tolerance factor (0.8–1)[27–31] and the octahedral factor (0.4–0.8).[27] In contrast to conventional chalcogenide QDs, Pb halide PQDs possess superior optoelectronic properties (e.g., high PLQY, facile band-gap tunability, narrow PL bandwidth) and processing versatility (e.g., simpler solution-based synthesis, lower manufacturing costs) without an additional electronic surface passivation layer.[18,24,32]

To obtain high crystallinity and unveil the quantum-confined properties in Pb halide PQDs, two solution-based synthesis approaches are commonly used in batch reactors: (1) the hot-injection method and (2) the ligand-assisted reprecipitation strategy (LARS).[33] In both synthesis techniques, several key reaction parameters, including reaction temperature, growth time, structure and concentrations of surface capping ligands, and precursor concentrations are varied to achieve monodisperse PQDs with different sizes and optoelectronic properties.[33,34] Conventionally, batch (i.e., flask-based) reactors have been utilized for fundamental and applied studies of colloidal QDs. However, the fast formation kinetics of Pb halide PQDs[1,35] may result in batch-to-batch variation, prolonged experimental times (heat-up/cool-down delays), size broadening in as-synthesized PQDs, and large-scale manufacturing difficulties in batch reactors.[36–38] Furthermore, non-uniform heat and mass transfer rates, irreproducible/uncontrolled mixing times, and lack of access to *in situ* characterization probes in batch reactors result in an unfavorable synthesis environment for Pb halide PQDs, making it difficult for all precursors to follow identical and consistent precursor conversion rates as well as nucleation and growth pathways.[36–38] Additionally, due to the PQD size broadening phenomenon observed in batch reactors, typically multi-stage size-selective purification/separation steps are required to achieve highly monodisperse QDs for characterization purposes.

The fast nucleation and growth kinetics of Pb halide PQDs[1,35] requires meticulous control over the massive colloidal synthesis parameter space to achieve high-quality Pb halide PQDs (i.e., high PLQY and narrow size distribution) with application-specific optoelectronic properties. Recently, microscale flow synthesis strategies have been successfully utilized as a reliable/reproducible synthesis technique for accelerated fundamental and applied studies of Pb halide PQDs.[39–53] The microscale flow synthesis field typically deals with studies of single- or multi-phase chemical reactions in micro- or millifluidic channels.[54–56] Microscale flow synthesis systems are characterized by low Reynolds (*Re*) number (Equation 1) and are mostly in the laminar regime:

$$\left(Re = \frac{\rho u D}{\eta}\right), \qquad \text{(Equation 1)}$$

where ρ, u, D, and η represent fluid density, flow velocity, channel diameter, and fluid viscosity, respectively. Figure 1 illustrates an overview of in-flow synthesis and characterization of Pb halide PQDs utilizing modular fluidic microprocessors. The microscale flow synthesis platforms utilized for the controlled synthesis of Pb halide PQDs typically consist of three main modules (Figure 1), including a precursor formulation module, a flow synthesis module (i.e., microfluidic reactor), and an *in situ* diagnostics module (inset of Figure 1). Microfluidic reactors offer several distinct advantages, compared with batch reactors, for Pb halide PQD synthesis: (1) enhanced heat and mass transfer rates (process intensification); (2) rapid and controllable precursor mixing time; (3) precise process control via automation; (4) reduced reagent

[1]Department of Chemical and Biomolecular Engineering, North Carolina State University, Raleigh, NC 27695, USA

[2]These authors contributed equally

*Correspondence: abolhasani@ncsu.edu

https://doi.org/10.1016/j.matt.2020.07.024

Please cite this article in press as: Abdel-Latif et al., Flow Synthesis of Metal Halide Perovskite Quantum Dots: From Rapid Parameter Space Mapping to AI-Guided Modular Manufacturing, Matter (2020), https://doi.org/10.1016/j.matt.2020.07.024

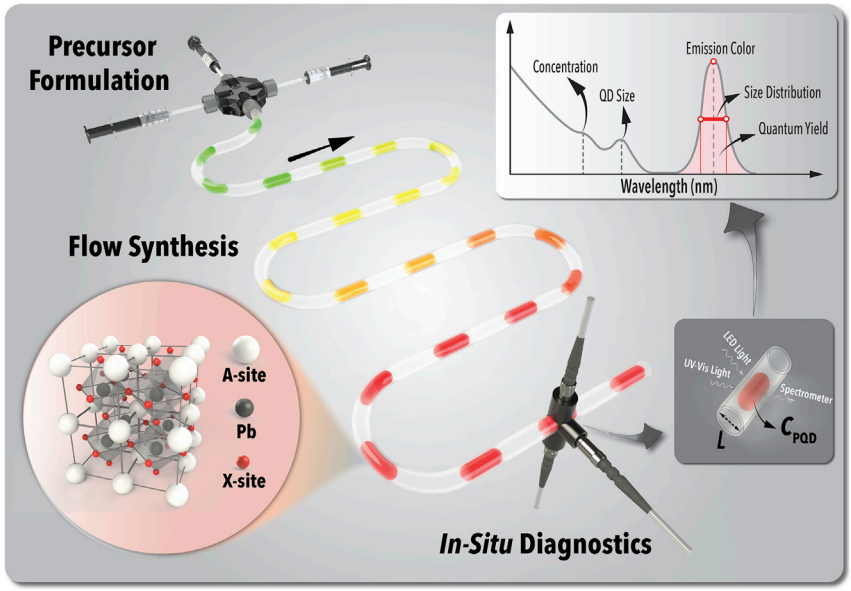

Figure 1. Schematic Illustration of In-Flow Synthesis and Characterization of Pb Halide PQDs
The illustration provides a schematic of a two-phase flow synthesis platform for controlled synthesis of Pb halide PQDs with precursor formulation, flow synthesis, and *in situ* diagnostics modules. The inset shows physicochemical and optoelectronic properties of Pb halide PQDs that can be obtained through *in situ* absorption and PL spectroscopy.

consumption while minimizing waste generation for exploratory studies of PQDs; (5) *in situ* and real-time PQD characterization; (6) high-throughput experimentation; and (7) accelerated parameter space mapping and optimization.[39–41,43,46,50,52,57–60] Consequently, microscale flow synthesis platforms enable time-, material-, and cost-efficient exploration and development of Pb halide PQDs.[39,40] Microscale flow synthesis platforms can also be employed for the elucidation of complex nucleation and growth mechanisms underlying the formation of PQDs. In addition to fundamental studies of formation of PQDs, flow synthesis strategies can be applied toward continuous manufacturing of high-quality PQDs with application-guided physicochemical and optoelectronic properties.[61]

The precursor chemistry, colloidal synthesis, post-synthesis modifications, and optoelectronic properties of Pb halide PQDs have previously been discussed in multiple excellent comprehensive review articles.[32,62–67] Moreover, the general characteristics of microfluidic reactors for synthesis of solution-processed nanomaterials have been previously reported elsewhere.[68–74]

In this review, we specifically focus on the rapidly growing microfluidic studies of Pb halide PQDs[39–53] and provide insights into how modular flow synthesis platforms can facilitate further advancements of this important class of semiconducting materials. In the next section, we briefly introduce the basics of microfluidic colloidal synthesis and discuss the important flow synthesis design parameters. We then discuss the main components of microscale flow synthesis platforms, essential for the controlled synthesis of Pb halide PQDs. Next, we provide an overview of the recent flow synthesis efforts focused on the colloidal synthesis, *in situ* characterization, post-synthesis processing, mechanistic studies, and optimization of Pb halide PQDs. We conclude by discussing the current challenges and potential future directions in this rapidly growing area of research. We hope that this review accelerates the adoption of

Please cite this article in press as: Abdel-Latif et al., Flow Synthesis of Metal Halide Perovskite Quantum Dots: From Rapid Parameter Space Mapping to AI-Guided Modular Manufacturing, Matter (2020), https://doi.org/10.1016/j.matt.2020.07.024

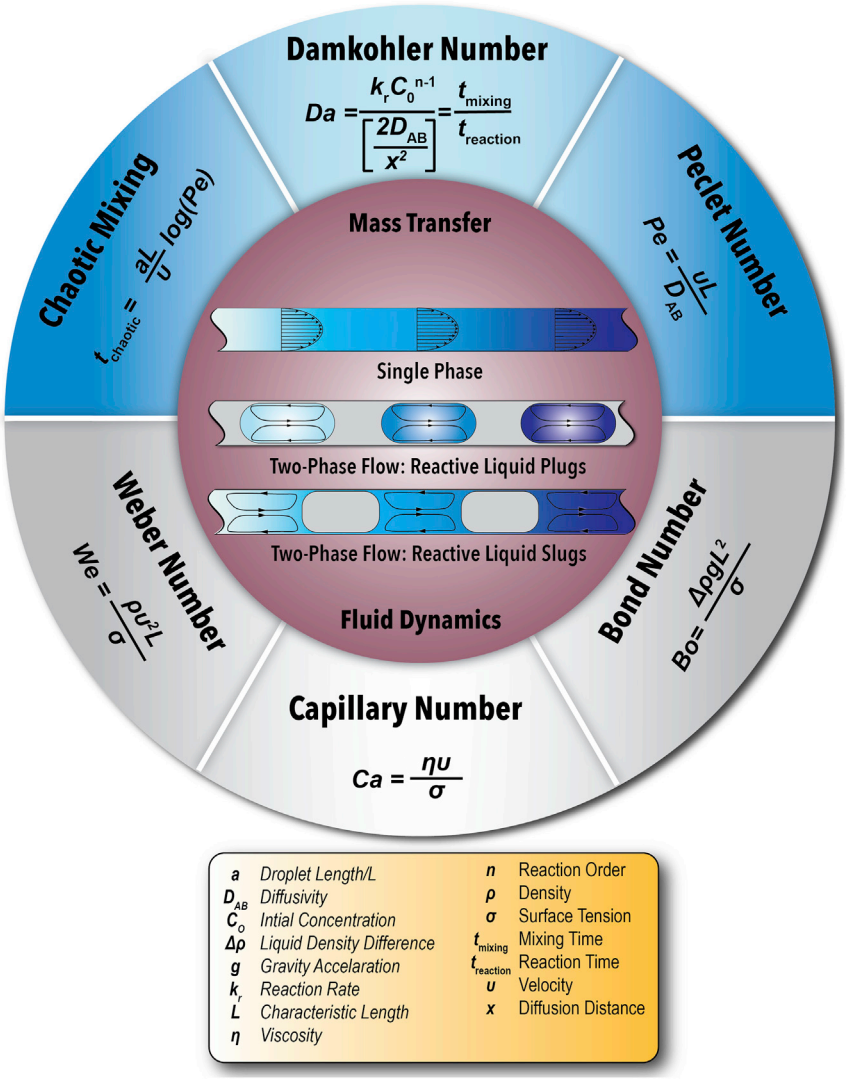

Figure 2. PQD Flow Synthesis Formats and Microreactor Design Parameters
The inset shows schematics of Pb halide PQD flow synthesis utilizing single- and two-phase flow formats.

flow synthesis techniques by materials scientists and enables a paradigm shift in the way colloidal PQDs are synthesized.

MICROFLUIDIC COLLOIDAL SYNTHESIS

Flow Format Matters: Single- versus Two-Phase Flow Synthesis

Single-phase flow material synthesis is the simplest form of colloidal synthesis and is normally sought after due to its relative design simplicity, ease of setup, and flow uniformity for multi-step sequential synthesis.[75–83] However, in-flow synthesis of Pb halide PQDs utilizing microscale single-phase flow format imposes two major drawbacks, namely axial dispersion[84] and fouling.[85] Axial dispersion in laminar flow is a fluid phenomenon characterized with a parabolic velocity profile (top channel, inset of Figure 2), where the PQD monomers are non-uniformly distributed radially and axially within the microchannel, thereby resulting in variable PQD growth rates along the flow direction. The dominance of axial dispersion in single-phase

Please cite this article in press as: Abdel-Latif et al., Flow Synthesis of Metal Halide Perovskite Quantum Dots: From Rapid Parameter Space Mapping to AI-Guided Modular Manufacturing, Matter (2020), https://doi.org/10.1016/j.matt.2020.07.024

flow synthesis constrains the mass transfer rate due to the slow diffusion rates, resulting in broad residence time distributions,[86] making it challenging for characterizing reactions with fast kinetics (e.g., Pb halide PQD synthesis). Furthermore, when utilizing single-phase flow format, the species (e.g., PQDs) near the microchannel wall reside longer in the flow reactor than the ones closer to the center of the microchannel (parabolic velocity profile).[86,87] The difference in the residence time of PQDs leaving the flow reactor for a fixed total flow rate directly translates into a wide PQD size distribution. Additionally, the direct contact of the reactive phase with the microchannel walls in the single-phase flow synthesis can result in reactor fouling due to deposition of PQDs on the surface of the microchannel walls during the nucleation or growth stages. The limitations of single-phase flow format for synthesis of colloidal PQDs can be eliminated by using an inert carrier phase, immiscible with the reactive phase to form two-phase flow (inset of Figure 2).

The introduction of a second phase results in the formation of axisymmetric recirculation zones that induce chaotic advection (enhanced mass transfer rates) inside the moving plugs or slugs (i.e., the reactive phase containing the PQDs),[88,89] resulting in narrowed residence time distribution.[86] The type of the carrier phase (i.e., inert fluid immiscible with the PQD mixture) and the surface force balance on the microchannel walls can result in formation of plugs (middle channel, inset of Figure 2) or slugs (bottom channel, inset of Figure 2) containing the PQD mixture. The choice of the carrier phase fluid (gas or liquid) in the two-phase flow material synthesis strategies depends on the PQD synthesis temperature and solvent. Perfluorinated oil is the preferred carrier fluid for relatively low-temperature synthesis (<180°C), as it can completely remove the contact between the reactive PQD phase (liquid plug) and the microchannel wall (no axial dispersion) in the case of Teflon as the microfluidic reactor substrate. Gas can be considered as the preferred carrier fluid choice for high-temperature PQD synthesis (>180°C) because higher temperatures can lead to increased PQD solvent miscibility with perfluorinated oil.[86] It has also been demonstrated that stable and uniform microscale gas-liquid flow can be achieved over a larger range of *Re* numbers[90,91] than liquid-liquid flow.[88,92] Moreover, the gas-liquid flow format does not require an additional separation step upon completion of the PQD synthesis in flow, since the gas phase can be easily separated from the reactive PQD phase. Despite the advantages of gas-liquid flow synthesis format, it suffers from the presence of a lubrication film around the gas phase that connects two successive reactive liquid slugs.[93–95] The presence of the lubrication film might lead to small axial dispersion (significantly lower than single-phase flow) and flow reactor fouling over extended periods of time due to the contact of the reactive PQD phase with the microchannel walls. Using a carrier phase fluid (e.g., perfluorinated oil) that completely separates the reactive PQD mixture (liquid plug) from the microchannel wall can address the potential axial dispersion and fouling issues of gas-liquid flow synthesis strategies.

Flow Synthesis Design Parameters

In this section, we discuss the important design parameters to consider for the in-flow synthesis of Pb halide PQDs. Flow synthesis design parameters provide a universal framework that guides researchers in the decision-making and flow reactor design process to achieve controlled flow synthesis of Pb halide PQDs. The relevant flow reactor design parameters for in-flow synthesis of PQDs can be divided into two categories, mass transfer and fluid dynamics design parameters, shown in Figure 2. Mass transfer design parameters include chaotic mixing time ($t_{chaotic}$), Damkohler number (*Da*), and Peclet number (*Pe*). Mass transfer parameters define the inter-droplet mass transport dynamics, ranging from precursor mixing efficiency to

Please cite this article in press as: Abdel-Latif et al., Flow Synthesis of Metal Halide Perovskite Quantum Dots: From Rapid Parameter Space Mapping to AI-Guided Modular Manufacturing, Matter (2020), https://doi.org/10.1016/j.matt.2020.07.024

mass transfer-controlled reaction kinetics. Fluid dynamics design parameters, including Weber number (*We*), Capillary number (*Ca*) and Bond number (*Bo*) provide an account of how the liquid phases interact with each other and the microchannel wall.

Mass Transfer Design Parameters

When designing a microscale flow synthesis platform for controlled synthesis of Pb halide PQDs, one of the important parameters that needs to be considered is *Da*, which relates the reaction rate to diffusion rate of precursors (Figure 2).[37,87] In the absence of rate information, *Da* can also be represented as the ratio of diffusion time to the reaction time. Diffusion time (t_{diff}) can be calculated using Equation 2,[96,97] and provides a good approximation for radial mixing across the microchannel wall in a single-phase flow system operating in the laminar regime:

$$t_{Diff} = \frac{x^2}{2D_{AB}}, \qquad \text{(Equation 2)}$$

where t_{Diff} is diffusion time, x is the characteristic diffusion length, and D_{AB} is the molecular diffusivity. *Da* can be used to explain the characteristics of PQD synthesis in flow. For $Da < 1$, the PQD synthesis is operating in a reaction-limited regime where the reaction rate is the limiting step. Alternatively, it means that chemical species (precursors and monomers) are mixed at a rate faster than they are being consumed, which leads to a homogeneous reaction environment for the PQD synthesis and thereby less heterogeneity in the resulting PQDs. $Da < 1$ is the desired range to conduct PQD synthesis for accurate mechanistic and rate-determining studies.[37] In contrast, when $Da > 1$, the PQD synthesis is considered to be mass transfer limited, or the mixing rate is not high enough to keep up with the fast formation kinetics. One of the causes for $Da > 1$ is slow mixing rates, which is very common in most batch systems, and is mostly the case for Pb halide PQD synthesis due to their fast intrinsic formation kinetics. Operating in the flow regime corresponding to $Da > 1$ is unfavorable, since it can result in an inhomogeneous synthesis environment and leads to inhomogeneity in the resulting PQDs. *Da* of a specific reaction can be lowered by either slowing the reaction rate or by improving the precursor mixing dynamics. The former is unfavorable in many cases, since it would involve changing the reaction temperature, pressure, or precursor concentrations, all of which have the possibility of changing the PQD nucleation and growth pathways and yields. The latter involves increasing the agitation in the reaction vessel or using smaller reactor dimensions to decrease the characteristic diffusion length (reducing diffusion time) (Equation 2). Two-phase microfluidic reactors are the case of drastically reducing the reaction vessel dimensions while providing enhanced mixing rates inside the moving reactive phase.

Pe relates two mass transfer mechanisms in the flow synthesis of PQDs: advection and diffusion. Typically, *Pe* values ranging between 10^3 and 10^5 are favorable for operating colloidal synthesis in a microfluidic reactor,[91] where mixing rates is considered to be fast enough while the average flow velocity is not excessively high to cause flow non-uniformity and instability.

The characteristic diffusion length (x) for single-phase flow can be approximated as half of the microchannel hydrodynamic diameter. However, in two-phase flow synthesis strategies, due to the formation of the recirculation patterns, the value of x reduces to a quarter of the microchannel hydrodynamic diameter. Thus, *Da* and *Pe* values corresponding to PQD synthesis can be reduced by one-fourth and one-half, respectively, when operating the synthesis under the two-phase flow format compared with the single-phase flow.

Please cite this article in press as: Abdel-Latif et al., Flow Synthesis of Metal Halide Perovskite Quantum Dots: From Rapid Parameter Space Mapping to AI-Guided Modular Manufacturing, Matter (2020), https://doi.org/10.1016/j.matt.2020.07.024

The mixing time inside the reactive liquid plug (or slug) moving within a microchannel can be approximated using the chaotic mixing time ($t_{chaotic}$) equation, which represents the effectiveness of serpentine microchannels in enhancing mixing rates within the reactive liquid plugs (Figure 2).[88,98,99] To achieve the desired *Da* regime while operating PQD synthesis in flow, care must be taken to ensure that $t_{chaotic}$ is fast enough such that the synthesis is operating under $Da < 1$. The mixing rates within the reactive plug (or slug) can be enhanced by: (1) minimizing the slug/plug length by manipulating the flow rate ratio of the two phases; (2) reducing the microchannel hydrodynamic diameter; and (3) increasing the average flow velocity.

Rational design of microscale flow synthesis strategies for controlled synthesis of high-quality Pb halide PQDs requires consideration of the flow reactor fluid dynamics in conjunction with the mass transfer design parameters. As shown in Figure 2, there are many design variables that affect both mass transfer and fluid dynamics design parameters. Thus, reasonable, optimal values should be attained for high-quality and reproducible flow synthesis of PQDs. For example, increasing the flow velocity enhances mass transfer rates (lower *Da* and $t_{chaotic}$, higher *Pe*) but also affects both *We* and *Ca* that are crucial to obtain a uniform, stable two-phase flow.

Fluid Dynamics Design Parameters

Ca represents the effect of viscous forces in relation to the surface tension between two immiscible fluids (liquid-liquid, gas-liquid). *Bo*, also referred to as Eötvös number, provides an indication of how dominant gravitational forces are relative to surface tension forces. Generally, to maintain and achieve a stable two-phase flow, viscous and surface tension forces should dominate the gravitational and inertial forces, which is reflected in *Ca* and *Bo* values less than 0.01 in circular microchannels.[100] *Ca* values higher than 0.01 (increasing the flow velocity or fluid viscosity) leads to undesirable annular flow format in most cases.[100] Values of *Bo* are more flexible than *Ca*, and can be increased as high as 0.3, while achieving stable two-phase flow. However, increasing *Bo* values close to 1 (e.g., by increasing the microchannel diameter), causes the lubrication film around the reactive PQD plugs to break due to the Laplace pressure gradient around the liquid plug that arises from increased effect of gravitational forces as the characteristic length scale increases.[101] *We* relates the fluid inertia to surface tension and is mostly used for two-phase flow systems. *We* is crucial for the stable formation of PQD plugs (or slugs) in two-phase flow synthesis, where $We < 1$ should be maintained to prevent a jetting flow.[102,103] For $We > 1$, the inertial forces become dominant, which hinders stable plug formation and leads to jetting.[102,103]

MICROFLUIDIC SYNTHESIS OF PB HALIDE PQDs: FROM MICROREACTOR DESIGN TO CONTINUOUS FLOW SYNTHESIS

In this section, we provide an overview of different modules of microscale flow synthesis platforms for controlled synthesis of Pb halide PQDs. Next, we discuss the *in situ* diagnostics toolkit currently available to flow synthesis platforms for high-throughput screening and accelerated synthesis science studies of Pb halide PQDs. The last part of this section is devoted to the recent efforts in low- and high-temperature flow synthesis of Pb halide PQDs, summarized in Figure 3.

Flow System Components

A typical microscale flow synthesis platform consists of four essential components, (1) precursor feeding (e.g., syringe pumps, pressure-driven pumps), (2) fluidic routing (e.g., tubing, fluidic connections, fittings, valves), (3) passive or active

Please cite this article in press as: Abdel-Latif et al., Flow Synthesis of Metal Halide Perovskite Quantum Dots: From Rapid Parameter Space Mapping to AI-Guided Modular Manufacturing, Matter (2020), https://doi.org/10.1016/j.matt.2020.07.024

Work	PQD				Synthesis Temperature		*In-situ* Diagnostic				Synthesis Parameters Studied						Reference
	$CsPbX_3$	$FAPbX_3$	$MAPbX_3$	$Cs_xFA_{1-x}PbX_3$	Low*	High*	PL	Absorption	PLQY	Fluorescence Lifetime	Synthesis Temperature	Pb-to-A Ratio	Ligand Effect	Br-to-Halide Ratio	Mixing Rate	Synthesis Kinetics	
Lignos et al., 2016	■					■	■	■			■	■		■		■	39
Epps et al., 2017	■				■		■	■							■		40
Maceiczyk et al., 2017		■				■	■		■		■	■		■		■	41
Lignos et al., 2018 (I)		■				■	■	■	■		■	■	■	■		■	42
Lignos et al., 2018 (II)				■		■	■	■	■		■			■		■	45
Liang et al., 2018			■		■		■		■					■			43
Bezinge et al., 2018				■		■	■				■	■		■			44
Abdel-Latif et al., 2019	■				■		■	■	■				■	■		■	46
Kerr et al., 2019	■				■		■								■		47
Zhang et al., 2019	■				■		■	■	■		■		■				52
Lignos et al., 2019	■					■	■		■	■	■	■		■			48
Kang et al., 2020	■					■	■		■		■			■			49
Li et al., 2020	■					■	■				■		■				50
Epps et al., 2020 (I)	■				■		■	■	■				■		■		51
Epps et al., 2020 (II)	■				■		■	■	■				■	■			52

Figure 3. Summary of Recent In-Flow Synthesis Science Studies of Pb Halide PQDs
The colored boxes imply that the specific parameter was included in the corresponding study. "Low*" and "High*" refer to synthesis temperatures lower and higher than 100°C, respectively.

micromixers, and (4) precursor and flow reactor heating (e.g., heating jackets, coils, oil bath) modules. *In situ* PQD characterization module (e.g., PL and UV-visible [UV-vis] absorption spectroscopy) is an optional component that can be readily integrated with microfluidic reactors.[70,72,73] A comprehensive review of different available precursor delivery mechanisms and micromixers is provided elsewhere.[72]

Microfluidic reactors can be classified into tube-/capillary-based and microfabricated reactors. Both types of microfluidic reactors have been utilized for the flow synthesis of Pb halide PQDs.[39–46,48–52,57,104–106] Tube and capillary-based microfluidic reactors utilizing either commercially available Teflon tubing or glass capillaries provide ease of microreactor assembly and rapid reconfigurability, while microfabricated reactors provide fully integrated processes within a small footprint (e.g., intensified mixing, rapid multi-precursor injection).[36,54,59,107,108]

Microfabricated flow reactors, utilizing reactive etching or additive manufacturing techniques, provide a compact design but are more expensive than capillary-/tube-based flow reactors, and in the case of fouling/clogging might have to be replaced with a new reactor. Li et al.[104] utilized additive manufacturing (three-dimensional printing using methacrylate photopolymer resin) to fabricate a microfluidic reactor for the continuous synthesis of hybrid organic-inorganic Pb halide PQDs (methylammonium Pb halide, $MAPbX_3$) with tunable size and emission colors. The flow rate of precursors and capillary diameters were adjusted to maintain an identical growth environment for the PQD monomers during the supersaturation step.

Compared with microfabricated flow reactors, tube-/capillary-based flow synthesis reactors, owing to their ease of reactor replacement and flexibility, have been more widely utilized for the in-flow studies of colloidal Pb halide nanostructures, including PQDs, nanowires, and nanoplatelets (NPLs).[39–46,48,49,51,57,104–106] For example, Zhang et al.[53] developed a tube-based flow reactor for the rapid synthesis of quantum-confined cesium lead bromide ($CsPbBr_3$) nanowires.

Please cite this article in press as: Abdel-Latif et al., Flow Synthesis of Metal Halide Perovskite Quantum Dots: From Rapid Parameter Space Mapping to AI-Guided Modular Manufacturing, Matter (2020), https://doi.org/10.1016/j.matt.2020.07.024

Polytetrafluoroethylene (PTFE) tubing with an off-the-shelf Y-junction micromixer was utilized to achieve controlled flow synthesis of $CsPbBr_3$ nanowires.[53] In a different study, Wei et al.[105] used a capillary-based flow reactor with a flow-focusing geometry for the continuous flow synthesis of fully inorganic Pb halide PQDs. The flow synthesis of Pb halide PQDs in this study was based on a flow-induced phase-separation strategy triggered by the polarity difference between the precursor solvent (dimethylformamide) and the reaction solvent (isopropanol).[105] A detailed discussion of the different microscale flow synthesis platforms developed for high-throughput screening and fundamental studies of Pb halide PQDs is provided in the section Microscale Flow Synthesis of Pb Halide PQDs.

In Situ Spectroscopy

Pb halide PQDs are an optically active class of materials and, therefore, optical spectroscopic techniques can be utilized to reveal their optoelectronic properties, including band-gap energy, peak emission energy, and PLQY. Microscale flow synthesis strategies allow for facile integration of multimodal *in situ* diagnostic modules with the fluidic microreactor (inset of Figure 1). Integration of *in situ* diagnostic probes with microscale flow synthesis reactors enables rapid colloidal synthesis parameter space exploration of Pb halide PQDs without the need for time-, labor-, and material-intensive conventional offline characterization techniques. Such *in situ* diagnostic modules enable access to important optical and structural characteristics of the PQDs synthesized in flow. UV-vis absorption and PL spectroscopy are the most utilized *in situ* characterization techniques that provide valuable insights into the properties of in-flow synthesized colloidal PQDs (inset of Figure 1). Recently, time-correlated single photon counting (TCSPC) has also been added to the diagnostic toolkit available to microscale flow synthesis platforms (Figure 4).[46,48,52] Figure 4 shows an exemplary set of PL (Figures 4A and 4D)[46,52] and absorption (Figures 4B and 4E)[46,52] spectra as well as PL decay (Figure 4C)[48] and PLQY (Figure 4F)[52] of in-flow synthesized Pb halide PQDs, acquired through *in situ* diagnostic modules.

The peak emission energy (or wavelength) corresponds to the emission color of the Pb halide PQDs (inset of Figure 1). The full width at half maximum (FWHM) of the PL spectra is an indicator of the homogeneity of PQD size or composition; a narrow FWHM is indicative of a homogeneous distribution.[109–111] Interquartile range can be used as a substitute for FWHM for multimodal fluorescence peaks.[50]

The *in situ* measured absorbance at a specific energy (or wavelength) in combination with the Beer-Lambert law ($A = \varepsilon C_{PQD} L$, where ε is the molar extinction coefficient, C_{PQD} is the PQD concentration, and L is the light path length in the microchannel) can be utilized to calculate the PQD concentration. To calculate C_{PQD} in a flow reactor under different synthesis conditions, accurate values of ε, independent of the PQD size, are required. De Roo et al.[112] have reported the experimentally measured values of ε for cesium lead bromide ($CsPbBr_3$) PQDs by complementing the UV-vis absorption spectra with inductively coupled plasma mass spectrometry. Furthermore, the first excitonic peak energy obtained from the absorption spectra of PQDs (inset of Figure 1), in combination with the effective mass approximation equation, can be utilized to calculate the size of PQDs synthesized in flow for each synthesis condition.[1,113] The correlation between the first excitonic peak and the PQD size can also be established through a series of UV-vis absorption spectroscopy measurements complemented with transmission electron microscopy (TEM) measurements.

Absorption and PL spectra of PQDs obtained *in situ* can also be utilized for quality assessment of the in-flow-synthesized PQDs through PLQY calculation. PLQY of

Please cite this article in press as: Abdel-Latif et al., Flow Synthesis of Metal Halide Perovskite Quantum Dots: From Rapid Parameter Space Mapping to AI-Guided Modular Manufacturing, Matter (2020), https://doi.org/10.1016/j.matt.2020.07.024

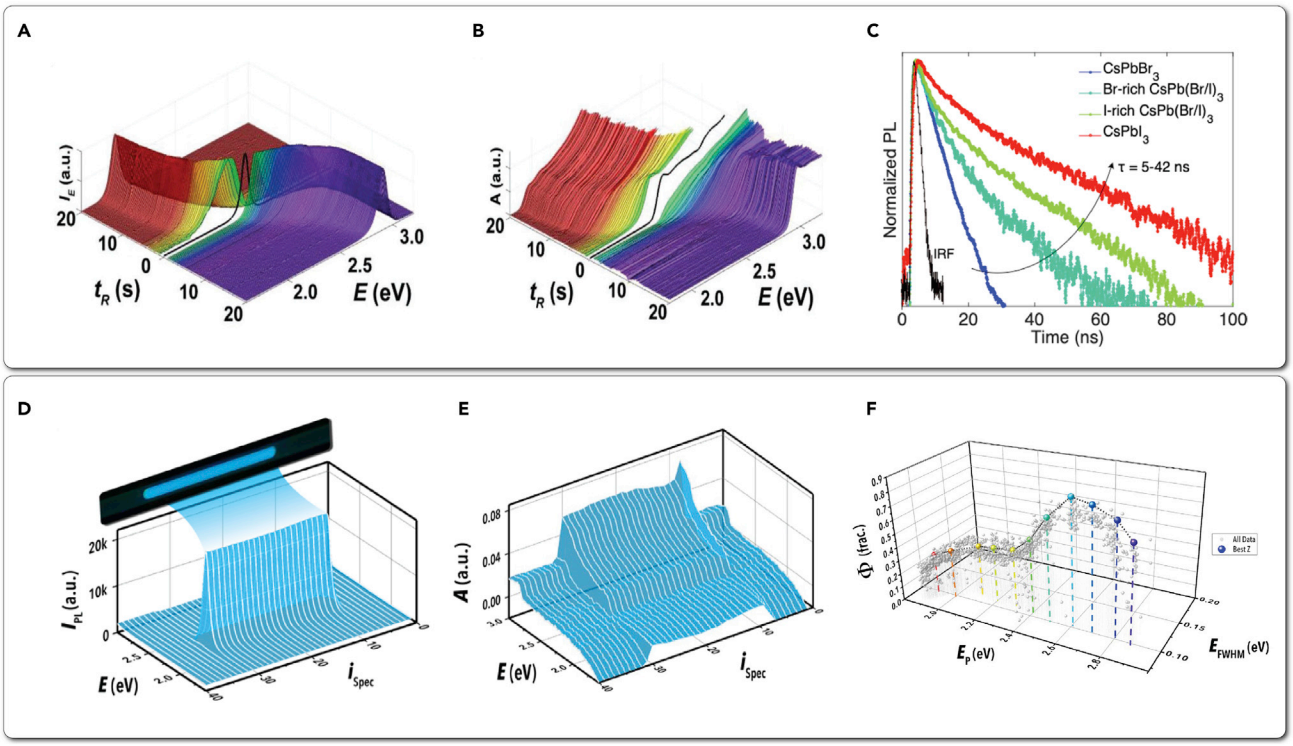

Figure 4. Examples of *In Situ* PL, Absorption, and Fluorescence Lifetime Spectroscopy Modules

(A and B) (A) High-resolution PL and (B) absorption spectra of Pb halide PQDs over the course of room-temperature halide exchange reactions (optical spectra of the starting $CsPbBr_3$ QDs is shown in black). Reproduced with permission from Abdel-Latif et al.[46] Copyright 2019, Wiley-VCH.

(C–E) (C) PL decay of $CsPbX_3$. Reproduced with permission from Lignos et al.[48] Copyright 2019, American Chemical Society. *In situ* obtained (D) PL and (E) absorption spectra of $CsPbCl_3$ PQDs in a two-phase flow reactor.

(F) AI-enabled construction of $CsPbX_3$ Pareto front through halide exchange reactions. Reproduced with permission from Epps et al.[52] Copyright 2020, Wiley-VCH.

PQDs indicates how efficient the synthesized nanocrystals are at emitting photons (energy loss through surface trap states) and is considered as one of the most important optoelectronic properties for downstream applications of Pb halide PQDs.

In addition to absorption and PL spectroscopy, fluorescence lifetime (FLIT) measurement of PQDs can also be integrated with microscale flow synthesis platforms. Recently, the TCSPC[48] technique has been successfully integrated with a microfluidic reactor, further expanding the available *in situ* diagnostic capabilities of microscale flow synthesis platforms for accelerated in-flow studies of PQDs. TCSPC can be utilized to reliably measure PLQY of in-flow synthesized PQDs irrespective of the sample concentration.

FLIT, enabled by TCSPC, provides an additional avenue to assess the quality and optoelectronic properties of Pb halide PQDs. Mono-exponential and multi-exponential decay behaviors correspond to high and low PLQY values of QDs, respectively.[114] FLIT also provides valuable insights into the stability of Pb halide PQDs, where surface defects and aging alter their PL lifetime.[114] Surface traps result in fast irreversible non-radiative trapping of charge carriers, which shortens the measured PL lifetime, while shallow trap states can extend PL lifetime by temporally trapping the charge carrier and delaying its return.[115] Furthermore, FLIT can be employed to evaluate the colloidal stability of Pb halide PQDs. Aggregation of PQDs facilitate the migration of exciton and charge carrier, which causes a red-shift in the transient

Please cite this article in press as: Abdel-Latif et al., Flow Synthesis of Metal Halide Perovskite Quantum Dots: From Rapid Parameter Space Mapping to AI-Guided Modular Manufacturing, Matter (2020), https://doi.org/10.1016/j.matt.2020.07.024

PL spectra and results in longer PL lifetime due to the buildup of electrons in the deepest states.[115,116] However, segregated PQDs should hamper carrier migration and minimize the number of deep traps, resulting in short PL lifetimes.[115] Lignos et al.[48] were the first to integrate FLIT with a microscale flow synthesis reactor as a diagnostics tool for accelerated in-flow studies of $CsPbX_3$ (X = Br, I) PQDs. FLIT exhibited a strong correlation with Pb:Cs ratio for all halide compositions tested. Utilizing the *in situ* FLIT measurement, it was reported that the average lifetime of $CsPbI_3$ PQDs decreased upon increasing the Pb:Cs ratio while an opposite behavior was observed for $CsPbBr_3$. Furthermore, the effect of temperature on the FLIT of Pb halide PQDs was studied. It was observed that the FLIT of $CsPbBr_3$ PQDs increased with temperature reaching a maximum at 180°C, due to confinement effect, then decreased with higher temperatures because high temperatures resulted in lower PL intensities. The same behavior was observed for $CsPbI_3$ PQDs. The type of halide used had a significant effect on FLIT whereby heavier halides resulted in longer FLITs due to the Fermi golden rule,[117] while lighter halides (and smaller PQDs) exhibited shorter FLIT.[118] However, the authors were cautious to point out that longer *in situ* measured FLIT of Pb halide PQDs with heavier halides might be also explained by the formation of metastable charge-separated states.[48,115]

Microscale Flow Synthesis of Pb Halide PQDs

Microscale flow synthesis platforms provide unique capabilities for reproducible and high-quality synthesis of colloidal Pb halide PQDs under a precisely controlled reaction environment. The in-flow synthesis of Pb halide PQDs can be broadly classified into two synthesis approaches, namely high-temperature and low-temperature synthesis, as shown in Figure 5. Both in-flow colloidal synthetic routes are discussed here.

Pb Halide PQDs: High-Temperature Synthesis

High-temperature, heat-up synthesis has been utilized as the most common approach for the in-flow synthesis of Pb halide PQDs.[39,41,42,44,45,48] Microscale flow synthesis of Pb halide PQDs was first introduced, in 2016, by Lignos et al.,[39] whereby a two-phase microfluidic reactor integrated with a multimodal *in situ* diagnostic probe (PL and UV-vis absorption spectroscopy) was utilized for the controlled synthesis of fully inorganic Pb halide PQDs (Figure 5A). The heat-up synthesis of Pb halide PQDs was performed through formation of a train of reactive phase plugs within an inert continuous phase (perfluorinated oil) at a multi-port fluidic junction at room temperature, followed by rapid in-flow heating in the heated section of the perfluoroalkoxy (PFA) tubing. The PFA tubing was coiled around a heating rod equipped with a thermocouple and temperature controller to monitor and tune the user-defined reaction temperature. Utilizing the developed microfluidic platform, the large colloidal synthesis parameter space associated with Pb halide PQDs (e.g., reaction temperatures, residence times, Pb:Cs and Pb:X molar ratios) was rapidly explored across the reaction time and temperature ranging from 0.1 s to 10 s and 120°C to 200°C, respectively. The mapped parameter space of Pb halide PQDs was then utilized for controlled synthesis of $CsPbX_3$ PQDs across the visible spectrum. Cesium-oleate (i.e., Cs_2CO_3 salt and oleic acid [OA] dissolved in 1-octadecene [ODE]) and PbX_2 (i.e., PbX_2 salt, OA, and oleylamine [OAm] dissolved in ODE) were used as the PQD precursors.

Microscale flow synthesis of Pb halide PQDs was also expanded to the in-flow synthesis of hybrid organic-inorganic PQDs.[41–45,104] Formamidinium Pb halide ($FAPbX_3$, X = Br, I) PQDs can extend the emission wavelength of PQDs to the near-infrared region of the electromagnetic spectrum.[41] Maceiczyk et al.[41] adapted the two-phase microfluidic

Please cite this article in press as: Abdel-Latif et al., Flow Synthesis of Metal Halide Perovskite Quantum Dots: From Rapid Parameter Space Mapping to AI-Guided Modular Manufacturing, Matter (2020), https://doi.org/10.1016/j.matt.2020.07.024

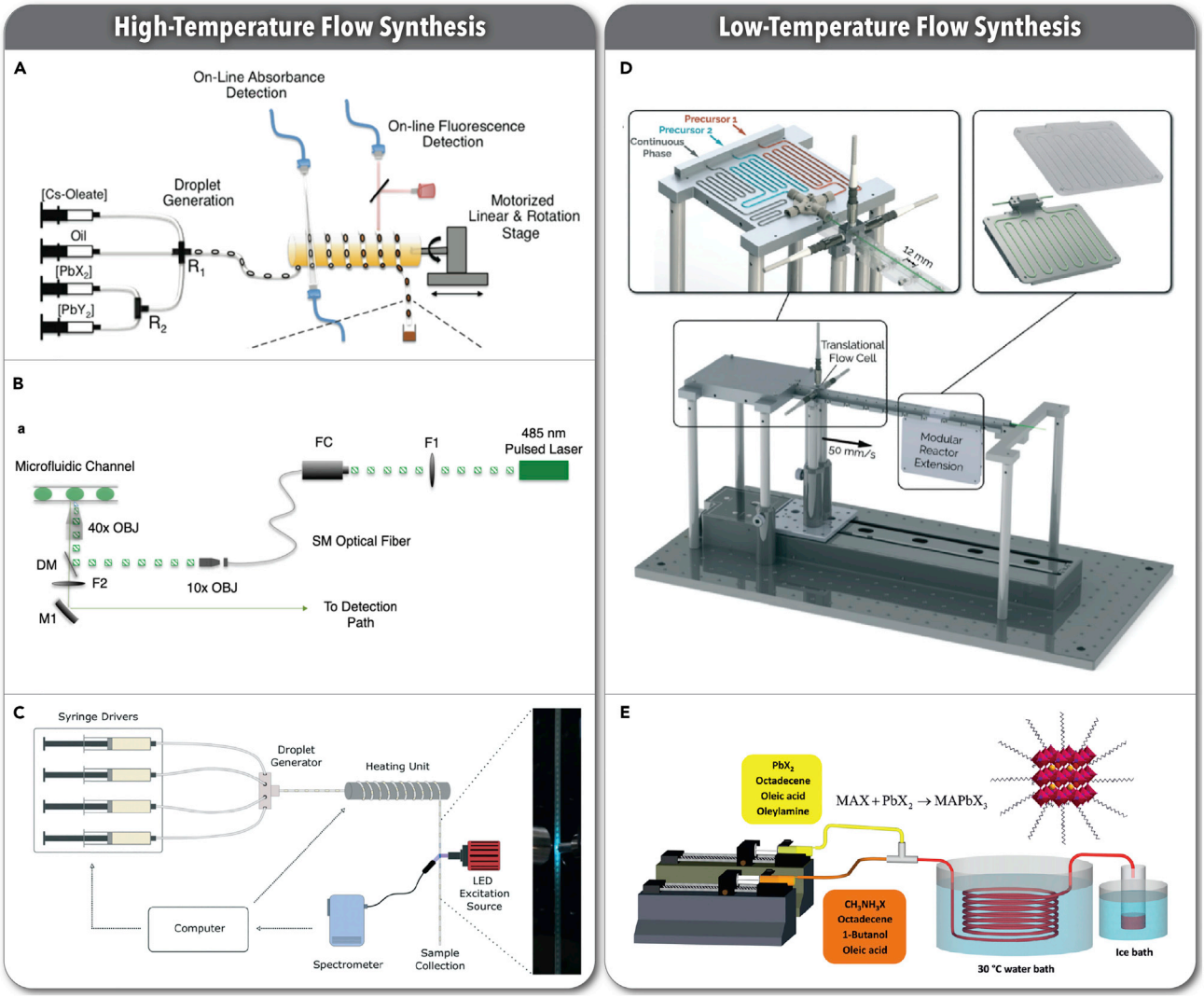

Figure 5. Microscale Flow Synthesis Platforms for High- and Low-Temperature Synthesis of Pb Halide PQDs

(A) A two-phase microfluidic platform equipped with *in situ* PL and UV-vis absorption spectroscopy module for high-temperature flow synthesis of fully inorganic $CsPbX_3$ PQDs. Reproduced with permission from Lignos et al.[39] Copyright 2016, American Chemical Society.

(B) The microfluidic platform from (A) integrated with TCSPC module for measuring PL lifetime of the in-flow synthesized $CsPbX_3$ PQDs. Reproduced with permission from Lignos et al.[48] Copyright 2019, American Chemical Society.

(C) A two-phase microfluidic platform for screening the interactive effects of temperature and ligand ratio on the optoelectronic properties of Pb halide PQDs. Reproduced with permission from Li et al.[50] Copyright 2020, The Royal Society of Chemistry.

(D) Low-temperature flow synthesis of $CsPbBr_3$ PQDs in a modular microfluidic setup integrated with translational *in situ* spectral diagnostic module. Reproduced with permission from Epps et al.[40] Copyright 2017, The Royal Society of Chemistry.

(E) Schematic illustration of the microfluidic platform for low-temperature flow synthesis of $MAPbX_3$ PQDs. Reproduced with permission from Liang et al.[43] Copyright 2018, The Royal Society of Chemistry.

platform developed by Lignos et al.[39] for accelerated studies of colloidal synthesis of $FAPbX_3$ PQDs. The reactive liquid plugs formed at room temperature were continuously flown into the heated section of PFA tubing with a residence time of up to 9 s while the temperature was adjusted between room temperature and 120°C. With highly tunable solution-processing offered through flow synthesis, the effect of FA and Pb halide precursors on the optoelectronic properties of the in-flow synthesized $FAPbX_3$ PQDs were rapidly explored *in situ* and provided mechanistic insights into the crystallization pathways of $FAPbX_3$ PQDs.

Please cite this article in press as: Abdel-Latif et al., Flow Synthesis of Metal Halide Perovskite Quantum Dots: From Rapid Parameter Space Mapping to AI-Guided Modular Manufacturing, Matter (2020), https://doi.org/10.1016/j.matt.2020.07.024

The structural stability of Pb halide PQDs can be further improved through incorporation of secondary monovalent cations and halides into the pristine Pb halide PQDs, i.e., multinary PQD structures composed of mixed A-site cations and halides.[45] A combinatorial screening of quinary PQD composition, $Cs_xFA_{1-x}Pb(Br_{1-y}I_y)_3$, was carried out in a two-phase microfluidic platform for a reaction time and temperature ranging from 0.1 s to 20 s and 25°C to 130°C, respectively.[45] FA-oleate, Cs-oleate, and two separate Pb halide precursor solutions were utilized as the Pb halide PQD precursors. *In situ* diagnostics coupled with X-ray diffraction revealed the formation of multinary Pb halide PQDs with high PLQYs up to 89%, narrow FWHM (below 40 nm), and high phase stability. It was also demonstrated that the incorporation of mixed small- and large-size A-site cations into the perovskite structure can optimally fill the available void space within the PQD crystal structure, which according to the Goldschmidt tolerance factor can significantly improve the phase stability of the resulting multinary Pb halide PQDs.[45]

The time- and temperature-dependent emissive properties of fully inorganic Pb halide PQDs were studied in flow utilizing a microfluidic platform integrated with an *in situ* TCSPC module (Figure 5B).[48] The average lifetime of the in-flow synthesized Pb halide PQDs was varied between 5 ns and 42 ns through tuning the precursor ratios (Pb:Cs and Br:I ratios).

One of the key components enabling high-quality and controlled synthesis of Pb halide PQDs is the structure and concentration of surface capping ligands (e.g., carboxylic acids, alkyl amines, phosphonates, or quaternary ammonium).[119] Microscale flow synthesis strategies can also be utilized for accelerated fundamental studies of the effect of surface capping ligands on the formation mechanism of Pb halide PQDs. In a recent study, a heat-up flow synthesis approach was employed within a two-phase microfluidic reactor (Figure 5C) for rapid evaluation of the effects of ligand structure, binary ligand ratio (alkyl amines to carboxylic acid), and reaction temperature on the quantum-confined properties of $CsPbBr_3$ PQDs.[50] Through systematic variation of the ligand structure (linear and branched ligands), the interactive effects of binary ligand ratios and reaction temperature on the resulting PL characteristics of $CsPbBr_3$ PQDs were explored.

Overall, high-temperature flow synthesis can lead to the manufacture of Pb halide PQDs with high crystallinity and phase stability.[66] However, the relatively high synthesis temperature limits the choice of inert carrier phase fluid and will require a detailed heat transfer calculations to ensure that uniform heat transfer across the microfluidic reactors is obtained.

Pb Halide PQDs: Low-Temperature Synthesis

As mentioned previously, low-temperature colloidal synthesis strategies (e.g., LARS) can also be employed for high-quality synthesis of Pb halide PQDs.[40,43,46,49,51] Epps et al.[40] developed a modular microscale flow synthesis platform, shown in Figure 5D, integrated with a custom-designed, multimodal *in situ* diagnostics module for accelerated colloidal synthesis studies of $CsPbBr_3$ PQDs at room temperature. Cs-Pb and bromide precursors were mixed using either an off-the-shelf T-junction or a custom-designed four-way junction to study the formation of $CsPbBr_3$ PQDs in single- and two-phase flow regimes, respectively. Furthermore, the translational *in situ* diagnostics module enabled decoupling of the flow-velocity-dependent mixing rates and residence times within the flow reactor. Utilizing the fully automated modular flow synthesis platform, kinetic tunability of $CsPbBr_3$ PQD synthesis within two-phase flow format was demonstrated. In a different low-temperature flow synthesis study,

Please cite this article in press as: Abdel-Latif et al., Flow Synthesis of Metal Halide Perovskite Quantum Dots: From Rapid Parameter Space Mapping to AI-Guided Modular Manufacturing, Matter (2020), https://doi.org/10.1016/j.matt.2020.07.024

Liang et al.[43] utilized a single-phase flow format (Figure 5E) for controlled synthesis of $MAPbX_3$ PQDs (X = Br, I). Pb halide precursor (PbX_2, X = Br and I, dissolved in ODE, OA, and OAm) and MA halide precursor (MAX, X = Br and I, dissolved in a mixture of n-butanol and ODE) were continuously delivered into a T-junction micromixer to form a single-phase flow reaction mixture flowing into a PTFE tubing at 30°C. Despite the relatively low reaction temperature, $MAPbX_3$ PQDs were formed within a few seconds after the mixing stage. Low-temperature synthesis generally produces PQDs with low crystallinity and phase stability compared with the high-temperature synthetic routes. However, they offer the advantage of facile solution-processing versatility in microscale flow synthesis platforms.[66]

Post-Processing of Pb Halide PQDs in Flow: Halide Exchange Reactions

Reversible post-synthesis halide exchange reactions using halide salts offer a facile processing route to precisely tune PQD optoelectronic properties.[18,46,120,121] For example, gradual replacement of bromide anions in $CsPbBr_3$ PQDs with chloride or iodide anions will change the PQD band gap (emission color), resulting in a blue- and red-shift, respectively. The extent of the halide exchange reaction within the PQD determines the final emission color of the resulting PQD. Utilizing the parent $CsPbBr_3$ PQD with a size-dependent peak emission wavelength ranging from 460 nm to 520 nm,[1] peak emission color can be readily tuned over the entire visible spectrum (400–700 nm).[18] Microscale flow synthesis strategies with *in situ* diagnostic modules, in addition to synthesis of Pb halide PQDs, have also been utilized to study the kinetics and fundamental mechanisms of halide exchange reactions in a controlled reaction environment.[46,49]

Abdel-Latif et al.[46] developed an automated modular flow synthesis platform for accelerated in-flow studies of halide exchange reactions of fully inorganic Pb halide PQDs. The developed gas-liquid two-phase flow synthesis platform was composed of a precursor formulation module, a novel static micromixer, a tube-based microreactor (fluorinated ethylene propylene [FEP]), a translational *in situ* diagnostic module adapted from Epps et al.,[40] and an optical flow-velocity meter for accurate residence time measurements (Figure 6A). Utilizing the multimodal, translational *in situ* diagnostic module, high-resolution PL and UV-vis absorption spectra of Pb halide PQDs throughout the halide exchange reaction were obtained at 76 distinct points along the flow reactor corresponding to different halide exchange reaction times (Figures 4A and 4B).

Epps et al.[52] developed a highly modular and adaptive microscale flow synthesis platform for intelligent exploration of halide exchange reactions of fully inorganic Pb halide PQDs with a multimodal *in situ* diagnostic module (PL and UV-vis absorption spectroscopy). The developed two-phase flow synthesis platform (liquid-liquid) enabled computer-controlled access to various concentrations of all halide exchange reaction precursors, including the starting $CsPbBr_3$ PQDs, halide salts, and surface capping ligands (OA and OAm). Three passive micromixers ensured a homogeneous reaction mixture within the formed reactive liquid plugs within the FEP tubing (Figure 6B).

Kang et al.[49] leveraged the rapid heat transfer rates of two-phase flow synthesis strategies for in-flow studies of high-temperature PQD halide exchange reactions. The developed two-stage flow synthesis platform (Figure 6C) consisted of two tube-based flow reactors for the controlled synthesis of $CsPbBr_3$ PQDs within the first flow reactor, followed by sequential halide exchange reactions in the second flow reactor at 150°C. Utilizing two-phase flow format, ODE as the reactive phase solvent,

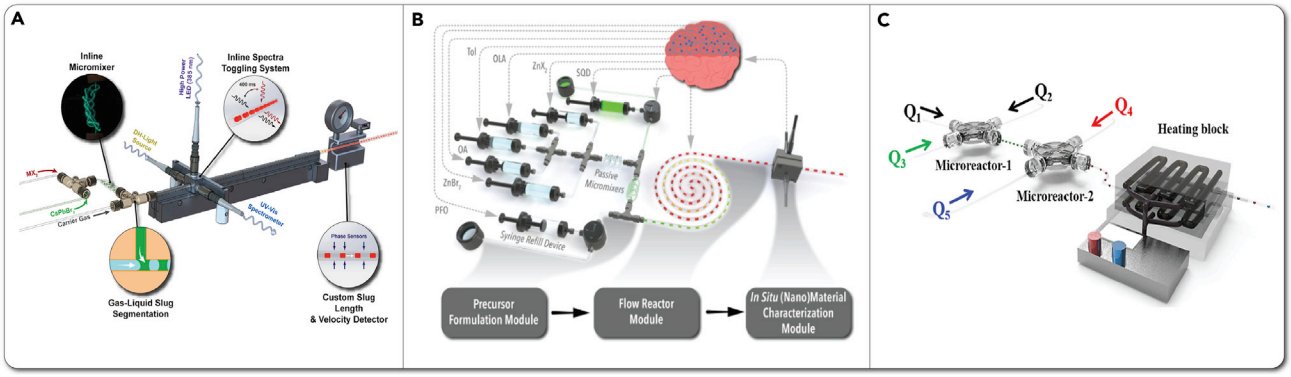

Figure 6. Microfluidic Platforms Developed for Post-synthesis Halide Exchange Reactions of Pb Halide PQDs

(A) Schematic of the automated modular microfluidic platform equipped with a passive micromixer, translational *in situ* spectral monitoring probe, and optical fluid velocity meter. Reproduced with permission from Abdel-Latif et al.[46] Copyright 2019, Wiley-VCH.

(B) Schematic illustration of the modular fluidic microprocessor for intelligent exploration and screening of PQD halide exchange reactions. Reproduced with permission from Epps et al.[52] Copyright 2020, Wiley-VCH.

(C) Schematic illustration of the two-stage flow synthesis platform developed for controlled sequential halide exchange reactions of Pb halide PQDs. Reproduced with permission from Kang et al.[49] Copyright 2020, Elsevier.

and perfluorinated oil as the carrier phase ensured excellent heat and mass transfer rates within the flow synthesis microreactor, resulting in high-quality halide-exchanged Pb halide PQDs. The developed flow synthesis platform was then utilized to study the effect of halide salt ratio to the parent $CsPbBr_3$ PQDs on the optoelectronic properties of the resulting halide-exchanged PQDs.

ACCELERATED FUNDAMENTAL STUDIES OF PB HALIDE PQDs IN FLOW

The major family of Pb halide PQDs studied using microscale flow synthesis strategies are $CsPbX_3$ (Figures 7A–7C),[39,40,46–53] $MAPbX_3$ (Figure 7D),[43] $FAPbX_3$ (Figure 7E),[41,42] and the multinary $Cs_xFA_{1-x}Pb(Br_{1-y}I_y)_3$ (Figure 7F) PQDs.[44,45] The key experimental parameters controlling the physicochemical and optoelectronic properties of Pb halide PQDs are (1) synthesis temperature, (2) Pb:A ratio, (3) Br:Cl/I ratio, (4) surface capping ligand structure, and (5) precursor conversion rate (i.e., mixing rate). In this section, we discuss the effect of these key experimental parameters, which can be automatically controlled during flow synthesis, on the resulting Pb halide PQDs.

Synthesis Temperature

Temperature has a profound impact on the nucleation and growth of PQDs.[53,122] Size and temperature are directly correlated, whereby increasing the colloidal synthesis temperature results in larger PQDs, causing a red-shift in the peak emission energy. However, the effect of temperature is not as straightforward for the other PQD properties such as FWHM, PLQY, and reaction yield.

The effect of synthesis temperature on the emission wavelength of fully inorganic Pb halide PQDs was studied in flow by Lignos et al.,[39] where the optimal reaction temperature range for synthesizing high-quality Pb halide PQDs (25 nm < FWHM < 45 nm) was found to be from 140°C to 200°C. It was also demonstrated that the emission wavelength increases with increasing temperature. In a different study,[50] utilizing a microscale flow synthesis platform, it was demonstrated that the synthesis temperature has a more profound effect on the optical properties of $CsPbBr_3$ PQDs than the type/combination of the ligand pair used in the synthesis. Furthermore,

Please cite this article in press as: Abdel-Latif et al., Flow Synthesis of Metal Halide Perovskite Quantum Dots: From Rapid Parameter Space Mapping to AI-Guided Modular Manufacturing, Matter (2020), https://doi.org/10.1016/j.matt.2020.07.024

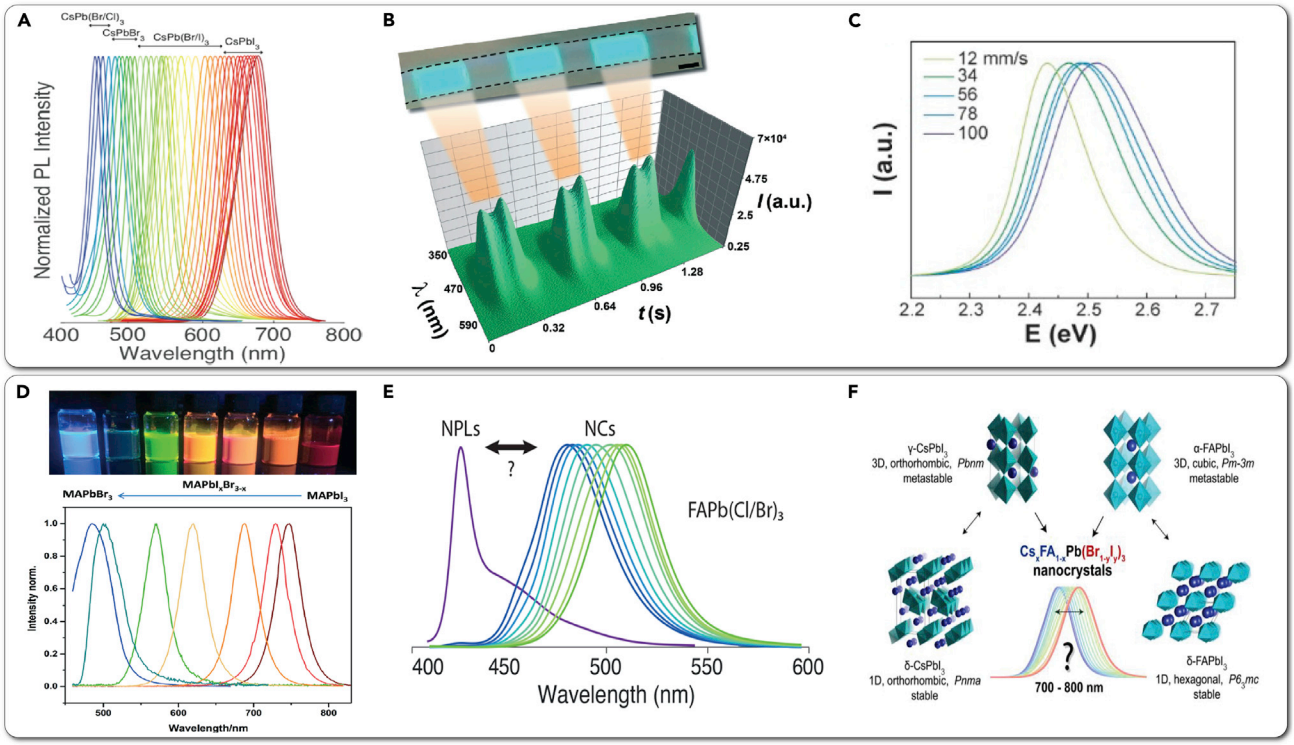

Figure 7. In-Flow Synthesis Science Studies of Pb Halide PQDs Utilizing *In Situ* PL Spectroscopy

(A) PL spectra of $CsPbX_3$ (X = Cl, Br, I) PQDs spanning the entire visible region. Reproduced with permission from Lignos et al.[39] Copyright 2016, American Chemical Society.

(B) Fluorescence image of a gas-liquid two-phase flow utilizing argon and toluene containing $CsPbBr_3$ PQDs with their corresponding PL spectra. Reproduced with permission from Epps et al.[40] Copyright 2017, The Royal Society of Chemistry.

(C) PL spectra of $CsPbBr_3$ PQDs as a function of the total average flow velocity. Reproduced with permission from Kerr et al.[47] Copyright 2019, The Royal Society of Chemistry.

(D) PL spectra of $MAPbX_3$ (X = Br, I) PQDs synthesized in flow. Reproduced with permission from Liang et al.[43] Copyright 2018, The Royal Society of Chemistry.

(E) Emission spectra of $FAPb(Cl/Br)_3$ PQDs spanning the blue-green region, which is representative of transition of nanoplatelets to nanocrystals. Reproduced with permission from Lignos et al.[42] Copyright 2018, American Chemical Society.

(F) PL spectra exhibiting the possibility of synthesizing Pb halide PQDs in the form of multinary $Cs_xFA_{1-x}Pb(Br_{1-y}I_y)_3$ that can emit in the near-infrared region. Reproduced with permission from Lignos et al.[45] Copyright 2018, American Chemical Society.

synthesis temperature plays an important role in determining the structure of the colloidal PQDs. Maceiczyk et al.,[41] utilizing a high-throughput microfluidic synthesis platform, observed that for $FAPbI_3$ lower synthesis temperatures favored the formation of NPLs, which was attributed to the decreased solubility of the chemical precursors in the solvent.[41,123] In addition, it was observed that higher synthesis temperatures diminished the tuning capability of the peak emission energy of $FAPb(Br/I)_3$.[41] Utilizing a similar flow synthesis platform, Lignos et al.[42] studied the effect of reaction temperature on the colloidal synthesis of $FAPb(Br/Cl)_3$, whereby the optimal synthesis temperature (minimum FWHM) for all Br:Cl ratios was identified to be 130°C. Lower synthesis temperatures resulted in broad PL spectra while higher synthesis temperatures led to PQD decomposition. In a different study,[45] the effect of reaction temperature on the flow synthesis of the multinary $Cs_xFA_{1-x}Pb(Br_{1-y}I_y)_3$ PQDs was explored. Over the range of temperatures tested (25°C–130°C), a $FAPbI_3$ emission peak (792 nm) was observed at room temperature. Furthermore, it was demonstrated the band-gap energy of the multinary Pb halide PQDs increased upon increasing the synthesis temperature, due to the incorporation of Cs into the PQD structure. TEM imaging was employed to rule out the

Please cite this article in press as: Abdel-Latif et al., Flow Synthesis of Metal Halide Perovskite Quantum Dots: From Rapid Parameter Space Mapping to AI-Guided Modular Manufacturing, Matter (2020), https://doi.org/10.1016/j.matt.2020.07.024

size-dependent blue-shift of the multinary PQDs. At synthesis temperatures higher than 110°C, a PL peak appeared at 700 nm, which was attributed to $CsPbI_3$. The optimized range of colloidal synthesis temperature (50°C–90°C) obtained rapidly by the automated microscale synthesis platform was then utilized for the subsequent in-flow screening studies.

Pb:A Ratio

Pb:A precursor ratios play a major role in the colloidal synthesis of Pb halide PQDs. For example, the competition between FA (A-site cation) and OAm, due to its acidity,[41] introduces additional dynamics into the growth pathway of $FAPbX_3$ (X = Br, Cl, I) PQDs.

Microscale flow synthesis platforms with the precise control over the PQD precursor concentrations enable systematic studies of the effect of precursor composition on the optoelectronic properties of Pb halide PQDs. Maceiczyk et al.[41] utilized a two-phase, liquid-liquid microfluidic platform to explore two different approaches of controlling FA:Pb ratio on the colloidal synthesis of $FAPbX_3$ (X = Br and I) PQDs. In the first approach, FA concentration was changed relative to PbI_2 concentration, while in the second approach all three ion concentrations were decoupled (i.e., the concentration of FA was changed relative to both Pb and I concentrations, separately). The former approach revealed that decreasing FA concentration in the $FAPbI_3$ synthesis favored the formation of smooth thin NPLs due to the competition between OAm and FA ions. Moreover, it was observed that increasing FA concentration caused a red-shift in the peak emission energy, a decrease in the FWHM, and the loss of high energy peaks in the PL spectra. A similar behavior was also observed for $FAPbBr_3$ with the only difference being that $FAPbBr_3$ was more susceptible to forming NPLs. The latter approach (separating all three ions) provided more control over the reaction stoichiometry. Low FA and Pb concentrations resulted in a mixture of NPLs that exhibited sharp emission peaks at 565 and 630 nm. However, higher FA and Pb concentrations suppressed the formation of NPLs and favored the growth of nanocubes with emission peak of 790 nm.

Lignos et al.[42] expanded the study conducted by Maceiczyk et al.[41] and focused on in-flow studies of $FAPb(Br/Cl)_3$. The high-throughput *in situ* studies conducted with a two-phase microfluidic reactor revealed that increasing Pb concentration (decreasing FA) resulted in formation of NPLs, which was in line with the results of the previous study.[41] Moreover, the rapid exploration of FA:Pb ratio with different Cl:Br ratios revealed a stable PL emission along with minimum FWHM for high FA:Pb ratios (5–10).[42] In another in-flow study of PQDs, it was found that for a mixed cation Pb iodide PQD ($Cs_xFA_{1-x}PbI_3$), at high FA:Pb ratios (>13) the crystalline structure tends to change from the black to yellow phase within hours.[45] PL tunability was also achieved for $Cs_xFA_{1-x}PbI_3$ PQDs with Cs loadings less than 10%. Utilizing a similar flow synthesis platform,[39] the optimal Pb:Cs ratios resulting in the smallest FWHM value (depending on the halide combination) for $CsPbX_3$ PQDs was rapidly obtained. The aforementioned in-flow studies of Pb:A ratio on the properties of Pb halide PQDs exemplify the unique capabilities of microscale flow synthesis techniques for accelerated synthesis science studies of complex colloidal systems.

Ligand Effect

Surface capping ligands play a crucial role in the colloidal stability, charge transport, and longevity of Pb halide PQDs. The presence and specific structure of capping ligands during the colloidal synthesis, or lack thereof, influences the growth rate and shape of colloidal QDs.[124,125] Surface capping ligands are usually coupled in an

Please cite this article in press as: Abdel-Latif et al., Flow Synthesis of Metal Halide Perovskite Quantum Dots: From Rapid Parameter Space Mapping to AI-Guided Modular Manufacturing, Matter (2020), https://doi.org/10.1016/j.matt.2020.07.024

acid-base pair to ensure charge neutrality on the PQD surface.[112,124,125] The most frequently utilized surface capping ligand pair is the OA-OAm pair. Despite their widespread utilization, the OA-OAm pair is not optimal for colloidal synthesis of high-quality Pb halide PQDs due to their labile nature and tendency to detach from the PQD surface,[32,112,126] leading to aggregation and colloidal instability.

Microscale flow synthesis strategies with *in situ* diagnostic capabilities can significantly accelerate the library screening and optimization of surface capping ligand composition in controlled synthesis or post-synthesis halide exchange of high-quality Pb halide PQDs.[42,46,50,51]

Lignos et al.[42] explored the effect of addition of free OA to the $FAPb(Br/Cl)_3$ synthesis mixture in flow. Excess OA suppressed the formation of PQDs and drove the reaction toward formation of NPLs with a single peak emission wavelength at 420 nm. It was shown that at higher OA:OAm ratios (>2:1), high yields of NPLs could be synthesized.

In a recent microfluidic study, Epps et al.[51] utilized an automated flow synthesis platform with a tunable precursor mixing time module to provide a comprehensive study of OA effect on the room-temperature synthesis of $CsPbBr_3$ PQDs. The volumetric fraction of OA was automatically varied from 1.8% to 6.7% in flow, and its impact on the peak emission wavelength, FWHM, PLQY, and concentration of $CsPbBr_3$ PQDs was monitored *in situ*. It was demonstrated that at higher mixing times (i.e., slower mixing rates), OA volume had a more significant impact on the PQD peak emission energy. Moreover, it was observed that reducing the precursor mixing times (i.e., faster mixing rates) resulted in improved FWHM values but worse PLQY of the in-flow synthesized $CsPbBr_3$ PQDs.

In a different study, a two-phase microfluidic platform was utilized to investigate the effect of ligand chain structure (linear versus branched) on the growth of $CsPbBr_3$ PQDs.[50] The tested ligands in this study included octylamine, octanoic acid, 2-ethylhexylamine, and 2-ethylhexanoic acid. This study showcased the utility of microscale flow synthesis strategies in highly efficient studies of a multi-variable multi-output system. Utilizing the developed flow synthesis platform integrated with *in situ* PL spectroscopy, 11 different temperatures with 11 different base:acid ligand ratio (i.e., 121 parameter combinations for each ligand set) were rapidly screened. For linear-linear ligand pairs, a small dependence of the median emission wavelength on the base:acid ratio was observed. However, the base:acid ratio had a significant effect on the PL intensity, where high PL intensities were obtained for low base:acid ratios at 110°C for $CsPbBr_3$ PQDs with a peak emission wavelength of 460 nm. An opposite trend was observed at 140°C for $CsPbBr_3$ PQDs with a peak emission wavelength of 497 nm, where high PL intensities were obtained at high base:acid ratios. Comparing the data across the four sets of ligand combinations revealed that (1) linear ligand combination exhibited a dependence on base:acid ratio while the branched combinations exhibited no dependence, and (2) using branched ligands restricts controllability over PQD growth or stabilizing small PQDs, whereby branched ligands tend to result in larger PQDs.

The in-flow studies of the impact of the OA-OAm pair surface capping ligands was also expanded to the halide exchange reactions of Pb halide PQDs. Utilizing a two-phase flow synthesis platform, integrated with a multimodal *in situ* diagnostic module (UV-vis absorption and PL spectroscopy), Abdel-Latif et al.[46] studied the impact of OA and OAm on the kinetics and extent of halide exchange reactions of

Please cite this article in press as: Abdel-Latif et al., Flow Synthesis of Metal Halide Perovskite Quantum Dots: From Rapid Parameter Space Mapping to AI-Guided Modular Manufacturing, Matter (2020), https://doi.org/10.1016/j.matt.2020.07.024

$CsPbBr_3$ PQDs. It was observed that ligand:solvent ratio had no effect on the equilibrium peak emission wavelength of the halide-exchanged PQDs. However, increasing the ligand:solvent ratio lowered the initial reaction rate irrespective of the halide salt source. The acid:total ligand ratio had a significant effect on the kinetics and the optical characteristics of the halide-exchanged PQDs. It was observed that OA was crucial for the colloidal stability of the iodide-exchanged $CsPbBr_3$ PQDs due to its role in stabilizing the PQD structure while chloride-exchanged $CsPbBr_3$ did not exhibit a need for OA for structure stabilization. Halide exchange reactions with low acid:total ligand ratios resulted in Pb halide PQDs with relatively low PLQYs, confirming the importance of acid:base ratio optimization needed for high-quality Pb halide PQDs.[46,112,124,125] Furthermore, acid:total ligand ratio did not have an effect on the equilibrium peak emission energy of the halide-exchanged PQDs.

Halide Composition

The direct implication of changing the halide composition (e.g., Br:Cl or Br:I ratio) in the colloidal synthesis of Pb halide PQDs is the change in their peak emission wavelength. $APb(Br/X)_3$ PQDs populated with Cl anions have emission colors in the blue-green region of the visible spectrum (400–510 nm) while I-rich $APb(Br/X)_3$ PQDs emit in the green-red region (510–780 nm). The Br:X (X = Cl, I) ratio can be manipulated either by changing their ratio in the starting precursors (one-pot synthesis) or through post-synthesis halide exchange reactions.[18,46,120,121] The rapid precursor tuning capability offered by microscale flow synthesis platforms enable fast exploration of the effect of Br:X (X = Cl, I) ratio on the optoelectronic properties of the in-flow synthesized Pb halide PQDs. For example, Lignos et al.[39] demonstrated in-flow synthesis of $CsPbX_3$ PQDs with PL emission over the entire visible range (410–700 nm) by simply varying the ratio between $PbBr_2$ and PbX_2 (X = Cl, I).

In addition to variation of emission wavelength, several flow synthesis studies revealed the effect of Br:Cl/I ratio on the PL intensity, FWHM, and the crystal structure of the Pb halide PQDs.[41,42,45,46] Maceiczyk et al.[41] explored the effect of varying I:Br ratio in flow on the properties of $FAPb(Br/I)_3$ perovskite nanostructures, and demonstrated controlled PL spectra tuning from green to infrared (530 to 790 nm, $FAPbBr_3$ to $FAPbI_3$, respectively). It was observed that low iodide (i.e., Br-rich) content diminished the PL intensity and increased the FWHM. The broadening of PL spectra was attributed to the tendency of Br-rich NPLs to phase separation.[41,127] The same microfluidic platform was then utilized to investigate the Br:Cl ratio effect on the $FAPb(Br/Cl)_3$ synthesis in two ways.[42] First, $PbBr_2$ and $PbCl_2$ were used as the Pb and halide sources. In the second approach, independent sources were used for all ions (i.e., Pb-oleate and oleylammonium halide as Pb and halide sources, respectively). The decoupling of the ions exhibited significant differences in the optical properties of the resulting Pb halide PQDs. The in-flow measured reaction rates for the independent ion sources were higher than the combined precursor scenario (i.e., PbX_2). Furthermore, three emission peaks were observed, two of which were attributed to NPL and one was related to PQD. The observed differences across two precursor sources were attributed to the ligand concentration disparity between the two approaches. In a different set of in-flow synthesis experiments utilizing the same microfluidic platform,[42] it was demonstrated that the peak emission wavelength of $FAPb(Br/Cl)_3$ could successfully be tuned between 465 nm and 520 nm by varying the Br:X (X = Cl, I) ratio, with the narrowest FWHM and the highest emission intensity obtained in Br-rich environments.

Utilizing a two-phase flow synthesis platform equipped with an *in situ* PL spectroscopy module,[45] the effect of Br anion addition to $Cs_xFA_{1-x}PbI_3$ PQDs on the stability

Please cite this article in press as: Abdel-Latif et al., Flow Synthesis of Metal Halide Perovskite Quantum Dots: From Rapid Parameter Space Mapping to AI-Guided Modular Manufacturing, Matter (2020), https://doi.org/10.1016/j.matt.2020.07.024

of the nanocrystal structure was explored. Through exploration of the FA:Pb (2.5–6) and Cs:Pb (0.01–0.04) ratios, it was demonstrated that Pb halide PQDs with the peak emission wavelength between 690 nm and 780 nm could be synthesized in flow. It was also concluded that the Br content did not alter the FWHM or the PL emission intensity of the organic-inorganic Pb halide PQDs. Furthermore, the Br content greater than 25% resulted in formation of additional perovskite structures (e.g., $FAPbBr_{1-y}I_y)_3$.

In addition to the critical role of Br:Cl/I ratio in one-pot synthesis of Pb halide PQDs, it plays an important role in band-gap tuning through halide exchange reactions. Utilizing a gas-liquid flow synthesis reactor, Abdel-Latif et al.[46] revealed that using lower Br:Cl/I ratios (i.e., higher concentration of halide salts) increases initial reaction rate and the extent of the band-gap shift while lowering PLQY and FWHM for both iodide- and chloride-exchanged PQDs.

Precursor Mixing Rate

Pb halide PQD synthesis is conventionally performed using a flask-based, hot-injection strategy, which severely impedes the *in situ* diagnostic probes used for such colloidal systems.[67,128,129] The facile integration of *in situ* diagnostic probes with microscale flow synthesis reactors provides a unique opportunity to explore the effect of precursor mixing rates on the early-stage nucleation and growth pathways of Pb halide PQDs by simply varying the average total flow velocity (i.e., *Pe*) of the precursors continuously fed into the flow reactors.

Precursor mixing rate can be further decoupled from nucleation and growth stages of colloidal QDs by exploiting the modular nature of microscale flow synthesis platforms. Modular flow reactors have been successfully deployed to separate precursor mixing, nucleation, and growth stages of colloidal QD synthesis (e.g., Pb sulfide) by utilizing different fluidic modules for each synthesis stage.[130] The advantages of using a separate module for each stage is the ability to independently control the temperature and residence time of each module and thereby systematically study the effect of precursor mixing, nucleation, and growth time/temperature in isolation. A modular flow synthesis platform provides the means to study the relatively fast synthesis of LHP QDs, whereby the residence time and temperature in each module (precursor mixing, nucleation, and growth) can be independently varied by simple module design modifications or total flow rate adjustments. The precise control over the precursor mixing time becomes crucial for low-temperature colloidal synthesis chemistries.

Epps et al.[40] utilized a modular two-phase flow synthesis platform to explore the effect of precursor mixing time on the optoelectronic properties of $CsPbBr_3$ PQDs through *in situ* absorption and PL spectroscopy. It was demonstrated that when utilizing a gas-liquid flow synthesis system, the early-stage precursor mixing dynamics greatly affects the nucleation and growth pathway of $CsPbBr_3$ PQDs, whereby faster mixing timescales (i.e., higher flow velocities) resulted in a blue-shift of the peak emission wavelength of the resulting PQDs. In a follow-up study, Epps et al.[51] developed an automated microfluidic platform utilizing two separate flow reactors connected with a sample loop for accelerated studies of the precursor formulation mixing time on the optical properties of $CsPbBr_3$ PQDs. It was observed that the precursor mixing time, for otherwise identical reaction conditions, had a significant effect on the PL and absorption spectra of the in-flow synthesized $CsPbBr_3$ PQDs. This study provided further insights into the underlying mechanisms for the batch-to-batch variation of Pb halide PQDs synthesized in batch reactors.

Please cite this article in press as: Abdel-Latif et al., Flow Synthesis of Metal Halide Perovskite Quantum Dots: From Rapid Parameter Space Mapping to AI-Guided Modular Manufacturing, Matter (2020), https://doi.org/10.1016/j.matt.2020.07.024

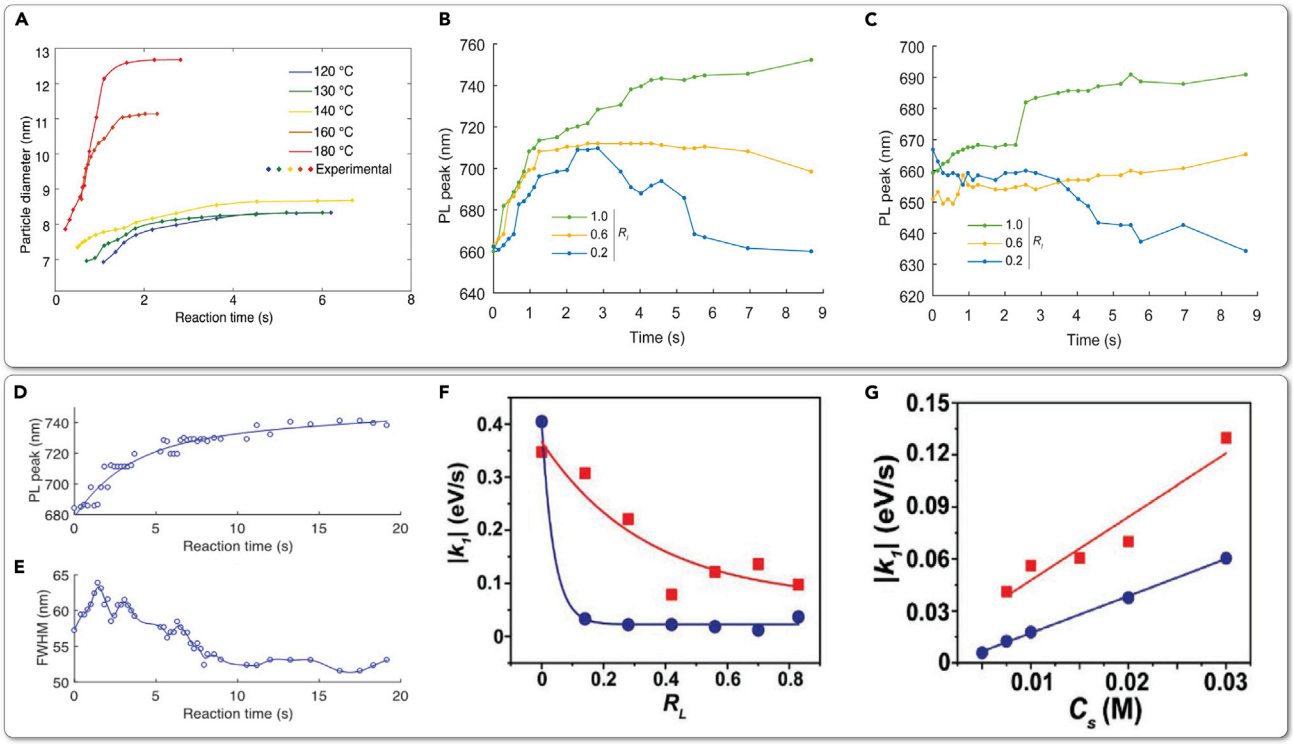

Figure 8. In-Flow Kinetic Studies of Pb Halide PQDs

(A–C) (A) Transient diameter evolution of $CsPbI_3$ PQDs at different in-flow synthesis temperatures. Reproduced with permission from Lignos et al.[39] Copyright 2016, American Chemical Society. Temporal evolution of PL peak wavelength during the in-flow synthesis of $FAPb(Br/I)_3$ at 80°C for (B) low and (C) high surfactant loadings. Reproduced with permission from Maceiczyk et al.[41] Copyright 2017, American Chemical Society.

(D–G) (D) Temporal evolution of normalized PL peak wavelength, and (E) FWHM for $CsFAPbI_3$ PQDs. Reproduced with permission from Lignos et al.[45] Copyright 2018, American Chemical Society. The initial halide exchange reaction rates, k_1, as a function of (F) ligands ratio(R_L) and (G) zinc halide concentration (C_s) for different metal halides (red: ZnI_2; blue: $ZnCl_2$).Reproduced with permission from Abdel-Latif et al.[46] Copyright 2019, Wiley-VCH.

Kinetic Studies of Pb Halide PQDs

In addition to the controlled, continuous manufacturing, microscale fluidic platforms have been exploited to unveil the nucleation and growth mechanism of Pb halide PQDs. In the first in-flow mechanistic study of colloidal PQDs, it was discovered that the nucleation pathway of Pb halide PQDs was similar to multinary metal chalcogenides but with faster reaction kinetics.[39] Figure 8A shows the size evolution of $CsPbI_3$ PQDs at various synthesis temperatures calculated from the *in situ* obtained absorption spectra.[39] As shown in Figure 8A, the Pb halide PQD diameter reaches a plateau between 2 s and 5 s, depending on the temperature, which demonstrates the fast inherent formation kinetics of fully inorganic Pb halide PQDs. Utilizing the same microscale flow synthesis platform, similar fast formation kinetics were observed for $FAPbX_3$ (X = Br, I).[39,41] Based on the obtained kinetic data, the formation of $FAPb(Br/I)_3$ had two successive stages. The first stage was postulated to be the nucleation of cube-shaped pure $FAPbI_3$ PQDs followed by the incorporation of bromide ions in the second stage.[41] Figures 8B and 8C present the trend of *in situ* obtained PL peak position during the flow synthesis of $FAPb(Br/I)_3$ PQDs at low and high concentrations of surface capping ligands, respectively. At low surface ligand loading (Figure 8B), all the kinetic curves reached a stable trend below 3 s, which indicated the presence of initially nucleated pure $FAPbI_3$ nanocrystals. Subsequent incorporation of bromide ions moves the PL peak positions to 660 nm. At higher surfactant loading (Figure 8C), the obtained kinetic data showed a similar trend, with faster incorporation of Br anions and concurrent formation of $FAPbBr_3$

Please cite this article in press as: Abdel-Latif et al., Flow Synthesis of Metal Halide Perovskite Quantum Dots: From Rapid Parameter Space Mapping to AI-Guided Modular Manufacturing, Matter (2020), https://doi.org/10.1016/j.matt.2020.07.024

PQDs. Utilizing the same two-phase flow microfluidic platform,[42] the challenging formation of Cl-rich $FAPb(Cl_{1-x}Br_x)_3$ PQDs due to the potential segregation of halide ions was studied in detail. Furthermore, the developed automated microfluidic platform was employed for kinetic studies of multinary mixed cation and anion Pb halide PQDs.[45] Figures 8D and 8E present the time evolution of PL peak and FWHM of quinary $CsFAPbI_3$ PQDs, where it follows a fast nucleation and growth kinetics similar to the first reported mechanism on fully inorganic Pb halide PQDs.[39,45]

As mentioned previously, one of the main characteristics of Pb halide PQDs is their facile band-gap tuning through halide exchange reactions.[18,46] Microscale flow synthesis platforms can be exploited to obtain a deeper understanding of the fundamental mechanisms governing the halide exchange reactions of Pb halide PQDs. A modular microfluidic platform was utilized for accelerated in-flow halide exchange kinetic studies of fully inorganic Pb halide PQDs.[46] The effects of ligand ratio (i.e., $R_L = V_{OA}/V_{OA} + V_{OAm}$, where V indicates volume) and zinc halide (i.e., $ZnCl_2$ and ZnI_2) concentration (C_s) on the kinetics of halide exchange reactions were rapidly explored (Figures 8F and 8G). It was observed that increasing the ligand ratio resulted in reducing the initial rate constant of the halide exchange reaction (Figure 8F), which was attributed to the limited diffusion of halide ions through the ligands attached to the surface of the Pb halide PQDs. Figure 8G shows the faster halide exchange kinetics due to increase in available zinc halide ions as the exchanging reagents. Utilizing the *in situ* obtained kinetic data through the modular microfluidic platform, a three-stage halide exchange reaction mechanism was proposed.[46]

The mechanistic studies in this section further substantiate microscale flow synthesis strategies as a powerful tool for gaining valuable insights into nanoscale phenomena that cannot be simply discovered by conventional flask-based synthesis techniques. Therefore, microscale flow synthesis platforms integrated with *in situ* diagnostic modules can provide materials scientists and chemists with a unique capability for accelerated fundamental and mechanistic studies of the early-stage nucleation and growth pathways of Pb halide PQDs as well as their post-synthesis halide exchange reactions.

ON-DEMAND FLOW SYNTHESIS OF PB HALIDE PQDs

Similarly to other colloidal nanoparticles, the synthesis of Pb halide PQDs with optimal optoelectronic properties and structural stability is a time-, material-, and labor-intensive practice that requires hundreds of experiments due to their highly complex multi-dimensional input parameter space.[44] Such a complex material design space combined with aforementioned challenges associated with traditional Edisonian flask-based material discovery, synthesis, and optimization strategies hinders further developments of high-priority Pb halide PQDs.[52] Despite the effectiveness of automated microfluidic platforms for high-throughput screening and controlled synthesis of Pb halide PQDs, they mostly rely on the knowledge, expertise, and materials selection of the operator for discovery, synthesis, and optimization. Exploration of the colloidal synthesis parameter space of each family of PQDs, without the aid of combinatorial designs, is costly in terms of time and chemical precursor consumption. Adoption of modular flow synthesis platforms integrated with *in situ* material diagnostic probes and controlled with optimization algorithms can significantly accelerate the development of next-generation colloidal QDs for targeted applications in chemical and energy technologies.[9,131–140] Specifically, integration of recently emerging artificial intelligence (AI) strategies (e.g.,

Please cite this article in press as: Abdel-Latif et al., Flow Synthesis of Metal Halide Perovskite Quantum Dots: From Rapid Parameter Space Mapping to AI-Guided Modular Manufacturing, Matter (2020), https://doi.org/10.1016/j.matt.2020.07.024

deep reinforcement learning)[141–147] with modular flow synthesis platforms can enable a paradigm shift in the synthesis, discovery, and manufacture of high-performance PQDs.

Despite the numerous advantages offered by AI-driven material synthesis and discovery strategies based on materials informatics, the field is still in its infancy and requires major advancements to reach the same level of cheminformatics in the field of pharmaceuticals. The challenges mainly revolve around the quantity and quality of the accessible data for rapid and reliable data mining. In contrast to the field of pharmaceuticals, where there is a large library of organic reactions readily available in the literature for data mining (>500,000), the scarce data availability in combination with the high degree of process dependency of colloidal QDs resulting in lab-to-lab, user-to-user, and batch-to-batch QD variation have hindered the convergence of the rapidly emerging AI strategies with colloidal nanoscience. The slow nature of the widely used flask-based colloidal synthesis methods is time-consuming and generates a limited amount of data, which impedes the development of a general representative model. Furthermore, databases with a wealth of information suffer from intrinsic biases and high variability,[148] which produces inaccurate and skewed QD synthesis models. Microscale flow synthesis strategies have the potential to address both aforementioned concerns by coupling their high-throughput screening and low chemical consumption with bias-eliminating statistical methods (i.e., design of experiments) to produce high-quality, in-house-generated QD synthesis data for AI model training and validation, thereby significantly accelerating the development of colloidal PQDs.

One of the key elements in achieving accurate, in-flow optimization of PQDs using the two-phase flow format is the correct estimation of the reactive phase's residence (reaction) time within the flow reactor. Optical measurement techniques, including digital cameras[149] or phase sensors,[150] can be utilized for real-time, accurate flow-velocity measurements of the reactive phase in a two-phase flow reactor. The *in situ* measured flow velocity can then be utilized to calculate the accurate residence times in the flow reactor. Kerr et al.[47] developed an optical technique using inexpensive phase sensors for facile *in situ* residence time measurements of two-phase flow in a tube-based microscale flow platform. The integration and automation of a low-cost and non-invasive optical velocity and length sensor (OVAL) module enabled rapid and precise measurement and control of residence time in the microscale flow reactor. The developed OVAL module was then applied toward mixing-controlled synthesis of $CsPbBr_3$ PQDs. Utilizing the OVAL module, integrated with a two-input, two-output fuzzy logic system, the velocity of PQD precursors was automatically varied from 12 mm/s to 100 mm/s, resulting in emission peak energy tunability of $CsPbBr_3$ PQDs from 2.43 eV to 2.52 eV.

Self-optimizing flow synthesis technologies can significantly expedite the development and manufacture of targeted PQDs with or without access to prior knowledge (i.e., PQD synthesis database). Bezinge et al.[44] integrated a two-phase microfluidic platform with a multi-parametric automated regression kriging interpolation (MARIA) algorithm for in-flow optimization of hybrid organic-inorganic Pb halide PQDs (Figure 9A). Employing the MARIA algorithm, the optimized synthesis protocol of $(Cs/FA)Pb(I/Br)_3$ and $(Rb/Cs/FA)Pb(I/Br)_3$ PQDs for peak emission wavelengths ranging from 560 nm to 680 nm was obtained automatically. In addition, the MARIA algorithm provided predictions of important optical properties of Pb halide PQDs, including FWHM and PL intensity. With approximately 20 iterations after the initial samples (16 experiments), MARIA can predict future reaction conditions with the

Please cite this article in press as: Abdel-Latif et al., Flow Synthesis of Metal Halide Perovskite Quantum Dots: From Rapid Parameter Space Mapping to AI-Guided Modular Manufacturing, Matter (2020), https://doi.org/10.1016/j.matt.2020.07.024

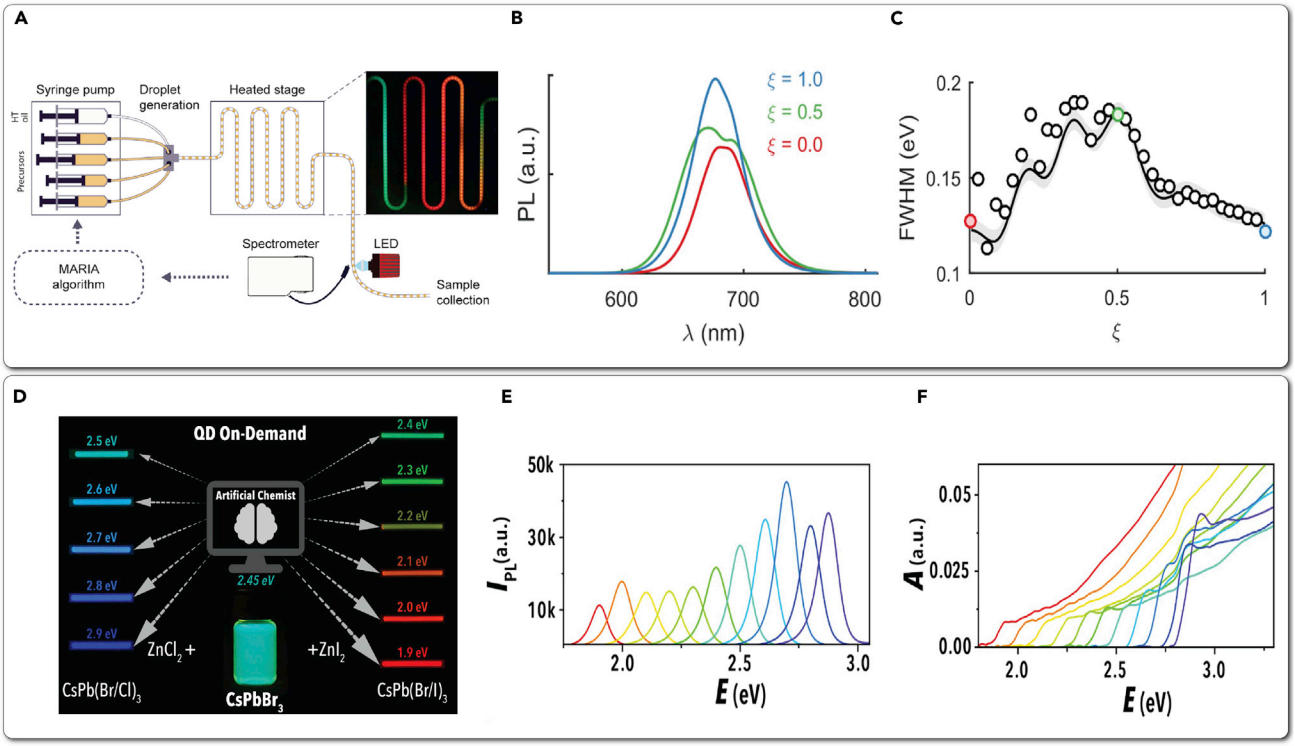

Figure 9. On-Demand Flow Synthesis of Pb Halide PQDs

(A) Schematic of the two-phase microfluidic platform integrated with MARIA algorithm for the in-flow synthesis of mixed cation Pb halide PQDs.

(B and C) (B) Experimentally obtained PL spectra for the predicted PQD synthetic routes using MARIA as a function a spatial coordinate (ξ) defined for the model's conditions, and (C) validation of the model predictions for FWHM values versus experimental data. (A), (B), and (C) reproduced with permission from Bezinge et al.[44] Copyright 2018, American Chemical Society.

(D) Accelerated and on-demand synthesis of Pb halide PQDs by the Artificial Chemist enabled through halide exchange reactions.

(E and F) (E) PL and (F) absorption spectra of 11 optimal PQD formulations autonomously synthesized by the Artificial Chemist. (D), (E), and (F) Reproduced with permission from Epps et al.[52] Copyright 2020, Wiley-VCH.

highest probability of obtaining the targeted wavelength, which corresponds to a total of 36 experimental runs (~1.5 h). Figure 9B shows an example of PL spectra of Pb halide PQDs obtained utilizing synthetic protocols predicted by MARIA as a function of a spatially weighted parameter ξ, defined in the algorithm. The predicted optoelectronic properties of Pb halide PQDs were then validated against the experimentally obtained data. Figure 9C shows an exemplary performance of the predicted values of FWHM using MARIA versus the experimentally obtained values for the peak emission wavelength of 680 nm. Utilizing the MARIA algorithm, the in-flow synthesis protocol of Pb halide PQDs was optimized based only on the peak emission wavelength.

One of the key properties defining the performance of colloidal PQDs in optoelectronic devices is their PLQY. The real-world applications of PQDs necessitate optimization (maximization) of their emitting photons measured through PLQY. In a recent study, Epps et al.[52] developed a novel *in situ* diagnostic probe capable of accurately measuring the PLQY of in-flow synthesized Pb halide PQDs without dilution through an innovative reduced-path-length strategy in a custom-designed flow cell module. The developed *in situ* diagnostic module was then integrated with a fully modular flow synthesis platform to achieve autonomous synthesis of Pb halide PQDs with application-guided optoelectronic properties. The developed self-driving PQD synthesizer, called Artificial Chemist, was directed by an AI-based optimization

Please cite this article in press as: Abdel-Latif et al., Flow Synthesis of Metal Halide Perovskite Quantum Dots: From Rapid Parameter Space Mapping to AI-Guided Modular Manufacturing, Matter (2020), https://doi.org/10.1016/j.matt.2020.07.024

algorithm (Bayesian optimization) to achieve on-demand synthesis and optimization of fully inorganic Pb halide PQDs (Figure 9D). Furthermore, the Artificial Chemist, for the first time, enabled simultaneous optimization of the emission bandwidth (E_{FWHM}) and PLQY (Φ) of Pb halide PQDs for any desired peak emission energy (E_P). It was demonstrated that the Artificial Chemist was capable of autonomously synthesizing high-quality Pb halide PQDs with or without access to prior knowledge. When the knowledge transfer of the archived PQD synthesis datasets from prior optimization runs were utilized for pre-training the surrogate model of the AI-based optimization algorithm, the optimized Pb halide PQDs were autonomously synthesized in less than 10 min for any desired emission color (Figures 9E and 9F). In addition to its highly modular design, the Artificial Chemist could autonomously be reconfigured from the discovery and process optimization mode to continuous manufacturing operation for large-scale synthesis of the autonomously optimized Pb halide PQDs. This proof-of-concept study highlighted the unique advantages of the convergence of microscale flow synthesis with state-of-the-art AI-based decision-making strategies for accelerated materials development. Further advancements of AI-guided PQD synthesis technologies can unlock novel formulations and manufacturing routes of next-generation, high-quality Pb halide PQDs toward achieving highly efficient and cost-effective optoelectronic devices.

OUTLOOK

As detailed throughout this review, microscale flow synthesis strategies have demonstrated their potential as a versatile and powerful tool for accelerated development of PQDs. Specifically, the in-flow studies of Pb halide PQDs have capitalized on the *in situ* characterization, rapid and accurate colloidal synthesis parameter space screening, and precisely controlled reaction environment capabilities of microfluidic platforms to boost the fundamental and applied studies of Pb halide PQDs. Despite the rapid progress of Pb halide PQDs over the last 5 years, further advancements in synthesis science and flow reactor engineering are needed to the realize the potential of PQDs as one of the leading semiconducting materials for next-generation, solution-processed optoelectronic devices. In this section, we discuss potential future directions for microfluidic studies of PQDs from (1) synthesis science and (2) flow reactor technological advancement perspectives.

Accelerated Synthesis Science Studies of PQDs Enabled by Microscale Flow Reactors

Microscale Flow Synthesis of Pb-Free Metal Halide PQDs

Despite the unique physicochemical and optoelectronic properties of Pb halide PQDs, the inherent toxicity of Pb is considered one of the major bottlenecks in widespread adoption of this exciting class of semiconducting materials. Recently, several studies have focused on reducing the amount of Pb present in PQDs toward achieving Pb-free PQDs with optoelectronic properties similar to their Pb halide counterparts. Currently, cation-doped (e.g., manganese, cadmium, zinc)[19,121,151] and Pb-free (i.e., substituting Pb with tin, germanium, indium, bismuth) PQDs have successfully been demonstrated at the batch scale with relatively poor optoelectronic properties (e.g., PLQY < 40%).[152] Employing microscale flow synthesis strategies integrated with *in situ* diagnostic probes can significantly accelerate the development of next-generation PQDs with reduced Pb content without sacrificing their structural stability and PLQY.

Colloidal Ligand Exchange

Surface capping ligands play a key role in the growth and colloidal stability of PQDs (see the section Ligand Effect).[153,154] Typically, the native surface capping ligands

Please cite this article in press as: Abdel-Latif et al., Flow Synthesis of Metal Halide Perovskite Quantum Dots: From Rapid Parameter Space Mapping to AI-Guided Modular Manufacturing, Matter (2020), https://doi.org/10.1016/j.matt.2020.07.024

used to reach the required size, shape, and structure of PQDs are ill suited for the targeted applications in chemical and energy technologies.[153,155] Thus, post-synthesis ligand exchange is typically performed to tailor the surface properties of PQDs (e.g., solubility, charge transport, solid-state packing density) for the targeted applications. For example, ligand exchange is a key step in fabrication of PQD-based solar cells, whereby the long-chain surface ligands are replaced with shorter, less bulky ligands to significantly improve charge transport throughout the device.[3,5,6] In addition, it has been demonstrated that PQD ligand exchange can enhance LED performance,[17] improve colloidal and structural stability,[156] and boost PLQY[3,17,32,156] of Pb halide PQDs, thus making ligand exchange an important process for the development of high-performance PQD-based optoelectronic devices.

Currently the majority of Pb halide PQD ligand exchange efforts are performed on thin films (i.e., solid-state ligand exchange).[3,5,6,157] Despite the considerable progress in performance of PQD-based devices,[2–6,130,158–160] solid-state ligand exchange processes suffer from time-, labor- and resource-intensive repetitive manual coating and washing steps.[157,161,162] Moreover, the Pb halide PQD thin film is prone to cracking after every solid-state ligand exchange cycle due to volume shrinkage caused by drying and ligand replacement,[153,162] leading to uneven surfaces that impede accurate data acquisition. Additionally, solvent polarity and ligand coordination ability affect the kinetics and mechanism of solid-state ligand exchange on the PQD surface.[153] To this extent, colloidal ligand exchange, also referred to as solution-phase ligand exchange,[155,163,164] has been explored as an alternative route to address the aforementioned challenges associated with solid-state ligand exchange of PQDs. Another reason that makes colloidal ligand exchange of PQDs an appealing surface engineering route is its compatibility with flow reactors with high-throughput screening capabilities, which can enable rapid exploration of the massive accessible parameter space of target capping ligand and solvent pairs for application-guided surface engineering of high-quality PQDs.

Flow Reactor Engineering: From Modular Components to Reconfigurable Operation

Intelligent Flow Synthesis Platforms

With the advent of modular flow synthesis reactors and rapidly growing AI strategies, the new generation of in-flow synthesis of PQDs should rely heavily on convergence of colloidal synthesis, flow reactor engineering, and AI to truly capitalize on the advantages of microscale fluidic handling technologies and the wealth of data made available through *in situ* diagnostics.[145,165] The new frontiers of PQD development efforts should focus on integration of materials informatics with highly reconfigurable flow synthesis reactors to achieve fully autonomous formulation discovery as well as time- and cost-effective process development and continuous manufacturing of next-generation, high-quality PQDs.[44,52]

In Situ *Material Diagnostics*

Despite the wealth of information made available through *in situ* spectroscopy techniques, acquiring accurate absorption spectra of Pb halide PQDs can be very challenging. As mentioned previously (see the section In Situ Spectroscopy), the UV-vis absorption spectra can be utilized for accelerated measurement of band-gap energy, average size, concentration, and PLQY of in-flow synthesized Pb halide PQDs. However, absorption (optical density) and PL intensity are linearly proportional to concentration only up to an optical density of 0.05,[166,167] where beyond this very low threshold inner filter effects emerge and breach the Beer-Lambert law.

Please cite this article in press as: Abdel-Latif et al., Flow Synthesis of Metal Halide Perovskite Quantum Dots: From Rapid Parameter Space Mapping to AI-Guided Modular Manufacturing, Matter (2020), https://doi.org/10.1016/j.matt.2020.07.024

Inner filter effects are manifested when the sample's optical density/concentration becomes high enough so that both the incident and emitted light (for fluorescent materials) are absorbed before reaching the detector.[166,168] Fluorescent materials with small Stokes shift (i.e., PQDs) are especially vulnerable to the inner filter effects.[166] Specifically, the inner filter problem presents itself in PLQY measurements, whereby the PL quenching effect reduces the PL intensity, resulting in a pseudo-diminished measured PLQY values. Sample concentration has an additional effect on the peak emission wavelength of highly fluorescent materials (i.e., PQDs), whereby higher sample concentrations result in a red-shift of the peak emission wavelength due to the reabsorption of the shorter wavelengths,[166,169] and sample dilution results in a blue-shift.[169] Although it has been suggested that the inner filter effect can be corrected mathematically, it requires a system-specific correlation and is only valid for a limited range of sample concentrations.[169] Furthermore, extreme dilution can severely strip the stabilizing surface capping ligands off the surface of ionic PQDs, resulting in PQD clustering.[112] Utilization of the spectra correction or the extreme dilution approach depends on the nature of the colloidal system as well as the flow reactor design.

Reducing the optical density to eliminate the inner filter effect and achieve accurate absorption and PL spectra of PQDs can be approached from a reaction/reactor design perspective. One approach is through reducing the concentration of the in-flow synthesized PQDs by dilution. Despite achieving reduced optical density, the in-flow PQD dilution approach suffers from (1) dilution-caused ligand detachment,[32,112,126] (2) PL variation (e.g., PQD dissolution),[166,169] and (3) requirements of extra equipment and solvents. Another strategy to lower the concentration of the as-synthesized PQDs in the microscale flow reactor is using diluted precursors.[46] Alternatively, the optical density of Pb halide PQDs can be reduced in flow through decreasing the effective photon path length within the flow cell (i.e., tube diameter, inset of Figure 1).[52]

Although *in situ* UV-vis absorption and PL spectroscopy techniques can provide a multitude of physicochemical and optoelectronic properties of the in-flow synthesized PQDs, they do not provide any information about the crystal structure and surface ligand population. Thus, future efforts should focus on integration of novel material diagnostic tools with microscale flow reactors to further enhance the fundamental understanding of the mechanisms governing the nucleation and growth pathways of colloidal Pb-based and Pb-free PQDs. The employed *in situ* diagnostic tools should be sensitive enough to detect small sample volumes and be reasonably fast to capture millisecond time scales.

Table 1 presents a list of suggested additions to the currently available *in situ* diagnostic toolkit of microscale flow synthesis reactors with references to their successful applications in non-PQD flow synthesis platforms.

End-to-End Continuous Manufacturing of Pb Halide PQDs

The ultimate goal of PQD flow synthesis strategies from the manufacturing perspective is to achieve a complete end-to-end continuous manufacturing route, guided by an AI-based decision-making strategy, for low-cost production of high-quality, application-ready PQDs without any manual intervention. To achieve this highly ambitious yet achievable goal, multiple novel flow technologies, including (1) automated Pb halide PQD precursor preparation, (2) controlled precursor formulation, (3) multi-step flow synthesis of Pb-based or Pb-free PQDs, (4) continuous purification of the as-synthesized PQDs, and (5) on-demand surface engineering of the purified

Please cite this article in press as: Abdel-Latif et al., Flow Synthesis of Metal Halide Perovskite Quantum Dots: From Rapid Parameter Space Mapping to AI-Guided Modular Manufacturing, Matter (2020), https://doi.org/10.1016/j.matt.2020.07.024

Table 1. Suggested Additions to the *In Situ* Diagnostics Toolkit of Microscale Flow Synthesis Platforms

Spectroscopic Method	PQD Relevance	Limitations	Previous Integration in Flow: References
X-ray diffraction	• PQD nanocrystal structure[1,21,170–172] • PQD formation and growth pathway[173–176]	• time-consuming[177] • accessibility	Marmirolli et al.,[173] Polte et al.,[174] Oyanagi et al.,[175] Sun et al.,[176] Chan et al.[178]
Nuclear magnetic resonance	• surface capping ligand characterization[112,125,179] • colloidal ligand exchange	• solvent switch • low sensitivity due to the small reactor/sample volumes used[172,180,181] • special flow coil requirement[182–184]	Bart et al.,[182] Gomez et al.,[183] Sans and Cronin,[184] Takahashi et al.,[185] Mompeán et al.[186]
Raman spectroscopy	structural transitions and phases[187–191]	high signal variations in microfluidic devices[192]	Jahn et al.,[192] März et al.,[193] Yazdi et al.,[194] Smith and Dent[195]

PQDs, must be developed. Furthermore, novel AI-guided multi-step synthesis planning (retrosynthesis) strategies dedicated to colloidal nanomaterials are needed to leverage and utilize live-streamed *in situ* diagnostic data after each synthesis step and manufacturing module to efficiently control the overall PQD manufacturing platform and remove the batch-to-batch variation problem.

Despite the aforementioned advantages of microfluidic systems for accelerating the pace of research and development of Pb halide PQDs, they typically suffer from relatively low manufacturing throughput. Development of a reliable and cost-effective end-to-end Pb halide PQD manufacturing scheme using flow synthesis reactors can significantly affect their adoption and utilization at the industrial scale.

The most commonly used strategy to increase the manufacturing throughput of continuous flow reactors is to increase the microchannel dimensions (diameter and length). However, increasing the microchannel diameter beyond a certain limit will nullify all the benefits incurred from using small dimensions (Figure 2).[38] Another approach to increase the flow synthesis throughput is through increasing the flow rates used in the microreactors. However, increased precursor flow rates will significantly increase the pressure drop and the required reactor length (to maintain the same residence time).

Scaling-out (i.e., numbering-up) is considered a viable alternative strategy for increasing the manufacturing throughput of microscale flow reactors while maintaining the characteristic transport length scales of a single-channel flow reactor.[196–198] The main challenge of the scaling-out technique utilizing the two-phase flow format is ensuring a uniform flow distribution across all flow reactor lines.[190,196,198–200] Recently, Wang et al.[201] have successfully demonstrated a scaled-out flow synthesis approach for continuous manufacturing of $CsPbBr_3$ PQDs at a throughput of 1 L/h with 10 nm and 5 nm variance of peak emission wavelength and FWHM across 16 parallel flow reactor lines, respectively. Future continuous manufacturing research efforts of Pb halide PQDs, utilizing two-phase flow formats, should focus on further improving the flow uniformity across parallel flow reactor lines to significantly reduce the variance of PQD optoelectronic properties manufactured in flow.

Scaling-out the PQD manufacturing introduces additional downstream engineering challenges. To achieve a reliable end-to-end continuous manufacturing route for

Please cite this article in press as: Abdel-Latif et al., Flow Synthesis of Metal Halide Perovskite Quantum Dots: From Rapid Parameter Space Mapping to AI-Guided Modular Manufacturing, Matter (2020), https://doi.org/10.1016/j.matt.2020.07.024

large-scale synthesis of high-quality Pb halide PQDs in addition to the scaled-out flow reactors, the phase separation, PQD purification, and surface engineering modules play a crucial role in ensuring that high quality and reaction yield of the as-synthesized PQDs are preserved while minimizing the manufacturing cost and the capital expenditure.

Upon completion of the colloidal PQD synthesis in flow, the carrier and the reactive phases should be separated to extract the desired product stream and recover the carrier phase for reuse in the PQD manufacturing platform. One of the promising approaches for facile phase separation of the carrier and the reactive phases in multi-phase flow synthesis is membrane-based liquid-liquid phase separation.[202] Porous Teflon membranes have been demonstrated to be successful for in-line separation of an oil-based carrier phase from a reactive phase containing colloidal nanomaterials, based on the difference in the affinity of the solvents to the porous Teflon membrane. Such an in-line, liquid-liquid phase-separation module would ensure continuous operation of a scaled-out multi-phase flow manufacturing process while separating the as-synthesized PQDs from the carrier phase for downstream purification.

The purification step of colloidal PQDs, similar to the other colloidal nanomaterials, is conducted using a multi-step washing protocol with an antisolvent (centrifugation). However, the relatively low throughput of the current antisolvent-based washing strategies necessitates development of more scalable PQD purification strategies with minimum surface damage (ligand removal). Cross-flow filtration,[203] gel-permeation chromatography,[204] and liquid-liquid extraction[205] are considered promising scalable nanocrystal purification strategies that can be adapted for continuous PQD purification in an end-to-end manufacturing platform. Microscale flow synthesis has also been demonstrated to be a viable scalable option for in-flow surface engineering (ligand exchange) of colloidal QDs.[206]

The aforementioned existing strategies offer a promising starting point for the development of an AI-guided, end-to-end continuous manufacturing route to achieve large-scale production (10–100 kg/day) of high-quality PQDs.

ACKNOWLEDGMENTS

The authors gratefully acknowledge the financial support provided by the National Science Foundation (award #1940959) and the UNC Research Opportunities Initiative (UNC-ROI) grant.

AUTHOR CONTRIBUTIONS

Conceptualization, K.A.-L., F.B., and M.A.; Writing – Original Draft, K.A.-L., F.B., and S.C.; Writing – Review & Editing, K.A.-L., F.B., and M.A.; Funding Acquisition, M.A.; Supervision, M.A.

REFERENCES

1. Protesescu, L., Yakunin, S., Bodnarchuk, M.I., Krieg, F., Caputo, R., Hendon, C.H., Yang, R.X., Walsh, A., and Kovalenko, M.V. (2015). Nanocrystals of cesium lead halide perovskites ($CsPbX_3$, X= Cl, Br, and I): novel optoelectronic materials showing bright emission with wide color gamut. Nano Lett. *15*, 3692–3696.

2. Fu, Y., Zhu, H., Chen, J., Hautzinger, M.P., Zhu, X.-Y., and Jin, S. (2019). Metal halide perovskite nanostructures for optoelectronic applications and the study of physical properties. Nat. Rev. Mater. *4*, 169–188.

3. Wheeler, L.M., Sanehira, E.M., Marshall, A.R., Schulz, P., Suri, M., Anderson, N.C., Christians, J.A., Nordlund, D., Sokaras, D., and Kroll, T. (2018). Targeted ligand-exchange chemistry on cesium lead halide perovskite quantum dots for high-efficiency photovoltaics. J. Am. Chem. Soc. *140*, 10504–10513.

4. Swarnkar, A., Marshall, A.R., Sanehira, E.M., Chernomordik, B.D., Moore, D.T., Christians, J.A., Chakrabarti, T., and Luther, J.M. (2016). Quantum dot-induced phase stabilization of α-$CsPbI_3$ perovskite for high-efficiency photovoltaics. Science *354*, 92–95.

5. Sanehira, E.M., Marshall, A.R., Christians, J.A., Harvey, S.P., Ciesielski, P.N., Wheeler, L.M., Schulz, P., Lin, L.Y., Beard, M.C., and Luther, J.M. (2017). Enhanced mobility $CsPbI_3$

quantum dot arrays for record-efficiency, high-voltage photovoltaic cells. Sci. Adv. *3*, eaao4204.

6. Xue, J., Lee, J.-W., Dai, Z., Wang, R., Nuryyeva, S., Liao, M.E., Chang, S.-Y., Meng, L., Meng, D., and Sun, P. (2018). Surface ligand management for stable $FAPbI_3$ perovskite quantum dot solar cells. Joule *2*, 1866–1878.

7. Yuan, J., Hazarika, A., Zhao, Q., Ling, X., Moot, T., Ma, W., and Luther, J.M. (2020). Metal halide perovskites in quantum dot solar cells: progress and prospects. Joule *4*, 1160–1185.

8. Li, G., Wang, H., Zhang, T., Mi, L., Zhang, Y., Zhang, Z., Zhang, W., and Jiang, Y. (2016). Solvent-polarity-engineered controllable synthesis of highly fluorescent cesium lead halide perovskite quantum dots and their use in white light-emitting diodes. Adv. Funct. Mater. *26*, 8478–8486.

9. Gao, L., Quan, L.N., de Arquer, F.P.G., Zhao, Y., Munir, R., Proppe, A., Quintero-Bermudez, R., Zou, C., Yang, Z., and Saidaminov, M.I. (2020). Efficient near-infrared light-emitting diodes based on quantum dots in layered perovskite. Nat. Photon. *14*, 227–233.

10. Song, J., Li, J., Li, X., Xu, L., Dong, Y., and Zeng, H. (2015). Quantum dot light-emitting diodes based on inorganic perovskite cesium lead halides ($CsPbX_3$). Adv. Mater. *27*, 7162–7167.

11. Bai, Z., and Zhong, H. (2015). Halide perovskite quantum dots: potential candidates for display technology. Sci. Bull. *60*, 1622–1624.

12. Zheng, W., Huang, P., Gong, Z., Tu, D., Xu, J., Zou, Q., Li, R., You, W., Bünzli, J.-C.G., and Chen, X. (2018). Near-infrared-triggered photon upconversion tuning in all-inorganic cesium lead halide perovskite quantum dots. Nat. Commun. *9*, https://doi.org/10.1038/s41467-018-05947-2.

13. Zhu, X., Lin, Y., Sun, Y., Beard, M.C., and Yan, Y. (2019). Lead-halide perovskites for photocatalytic α-alkylation of aldehydes. J. Am. Chem. Soc. *141*, 733–738.

14. Xu, Y.-F., Yang, M.-Z., Chen, B.-X., Wang, X.-D., Chen, H.-Y., Kuang, D.-B., and Su, C.-Y. (2017). A $CsPbBr_3$ perovskite quantum dot/graphene oxide composite for photocatalytic CO_2 reduction. J. Am. Chem. Soc. *139*, 5660–5663.

15. Wu, H., Li, X., Tung, C., and Wu, L. (2019). Semiconductor quantum dots: an emerging candidate for CO_2 photoreduction. Adv. Mater. *31*, 1900709.

16. Bao, C., Yang, J., Bai, S., Xu, W., Yan, Z., Xu, Q., Liu, J., Zhang, W., and Gao, F. (2018). High performance and stable all-inorganic metal halide perovskite-based photodetectors for optical communication applications. Adv. Mater. *30*, 1803422.

17. Pan, J., Quan, L.N., Zhao, Y., Peng, W., Murali, B., Sarmah, S.P., Yuan, M., Sinatra, L., Alyami, N.M., and Liu, J. (2016). Highly efficient perovskite-quantum-dot light-emitting diodes by surface engineering. Adv. Mater. *28*, 8718–8725.

18. Nedelcu, G., Protesescu, L., Yakunin, S., Bodnarchuk, M.I., Grotevent, M.J., and Kovalenko, M.V. (2015). Fast anion-exchange in highly luminescent nanocrystals of cesium lead halide perovskites ($CsPbX_3$, X = Cl, Br, I). Nano Lett. *15*, 5635–5640.

19. Swarnkar, A., Ravi, V.K., and Nag, A. (2017). Beyond colloidal cesium lead halide perovskite nanocrystals: analogous metal halides and doping. ACS Energy Lett. *2*, 1089–1098.

20. Aldakov, D., and Reiss, P. (2019). Safer-by-design fluorescent nanocrystals: metal halide perovskites vs semiconductor quantum dots. J. Phys. Chem. C *123*, 12527–12541.

21. Wei, S., Yang, Y., Kang, X., Wang, L., Huang, L., and Pan, D. (2016). Room-temperature and gram-scale synthesis of $CsPbX_3$ (X= Cl, Br, I) perovskite nanocrystals with 50-85% photoluminescence quantum yields. Chem. Commun. *52*, 7265–7268.

22. Fabini, D.H., Labram, J.G., Lehner, A.J., Bechtel, J.S., Evans, H.A., Van der Ven, A., Wudl, F., Chabinyc, M.L., and Seshadri, R. (2017). Main-group halide semiconductors derived from perovskite: distinguishing chemical, structural, and electronic aspects. Inorg. Chem. *56*, 11–25.

23. Ten Brinck, S., and Infante, I. (2016). Surface termination, morphology, and bright photoluminescence of cesium lead halide perovskite nanocrystals. ACS Energy Lett. *1*, 1266–1272.

24. Schmidt, L.C., Pertegás, A., González-Carrero, S., Malinkiewicz, O., Agouram, S., Minguez Espallargas, G., Bolink, H.J., Galian, R.E., and Perez-Prieto, J. (2014). Nontemplate synthesis of $CH_3NH_3PbBr_3$ perovskite nanoparticles. J. Am. Chem. Soc. *136*, 850–853.

25. Kang, J., and Wang, L.-W. (2017). High defect tolerance in lead halide perovskite $CsPbBr_3$. J. Phys. Chem. Lett. *8*, 489–493.

26. Guo, Y., Wang, Q., and Saidi, W.A. (2017). Structural stabilities and electronic properties of high-angle grain boundaries in perovskite cesium lead halides. J. Phys. Chem. C *121*, 1715–1722.

27. Li, C., Lu, X., Ding, W., Feng, L., Gao, Y., and Guo, Z. (2008). Formability of ABX_3 (X= F, Cl, Br, I) halide perovskites. Acta Crystallogr. Sect. B Struct. Sci. *64*, 702–707.

28. Carpenter, M.A., and Howard, C.J. (2009). Symmetry rules and strain/order-parameter relationships for coupling between octahedral tilting and cooperative Jahn–Teller transitions in ABX_3 perovskites. I. Theory. Acta Crystallogr. Sect. B Struct. Sci. *65*, 134–146.

29. Li, Z., Yang, M., Park, J.-S., Wei, S.-H., Berry, J.J., and Zhu, K. (2016). Stabilizing perovskite structures by tuning tolerance factor: formation of formamidinium and cesium lead iodide solid-state alloys. Chem. Mater. *28*, 284–292.

30. Huang, H., Bodnarchuk, M.I., Kershaw, S.V., Kovalenko, M.V., and Rogach, A.L. (2017). Lead halide perovskite nanocrystals in the research spotlight: stability and defect tolerance. ACS Energy Lett. *2*, 2071–2083.

31. Saparov, B., and Mitzi, D.B. (2016). Organic–inorganic perovskites: structural versatility for functional materials design. Chem. Rev. *116*, 4558–4596.

32. Akkerman, Q.A., Rainò, G., Kovalenko, M.V., and Manna, L. (2018). Genesis, challenges and opportunities for colloidal lead halide perovskite nanocrystals. Nat. Mater. *17*, 394–405.

33. Fu, P., Shan, Q., Shang, Y., Song, J., Zeng, H., Ning, Z., and Gong, J. (2017). Perovskite nanocrystals: synthesis, properties and applications. Sci. Bull. *62*, 369–380.

34. Dong, Y., Zhao, Y., Zhang, S., Dai, Y., Liu, L., Li, Y., and Chen, Q. (2018). Recent advances toward practical use of halide perovskite nanocrystals. J. Mater. Chem. A *6*, 21729–21746.

35. Hou, S., Guo, Y., Tang, Y., and Quan, Q. (2017). Synthesis and stabilization of colloidal perovskite nanocrystals by multidentate polymer micelles. ACS Appl. Mater. Interfaces *9*, 18417–18422.

36. Marre, S., and Jensen, K.F. (2010). Synthesis of micro and nanostructures in microfluidic systems. Chem. Soc. Rev. *39*, 1183–1202.

37. Hartman, R.L., McMullen, J.P., and Jensen, K.F. (2011). Deciding whether to go with the flow: evaluating the merits of flow reactors for synthesis. Angew. Chemie Int. Ed. *50*, 7502–7519.

38. Zhang, L., and Xia, Y. (2014). Scaling up the production of colloidal nanocrystals: should we increase or decrease the reaction volume? Adv. Mater. *26*, 2600–2606.

39. Lignos, I., Stavrakis, S., Nedelcu, G., Protesescu, L., deMello, A.J., and Kovalenko, M.V. (2016). Synthesis of cesium lead halide perovskite nanocrystals in a droplet-based microfluidic platform: fast parametric space mapping. Nano Lett. *16*, 1869–1877.

40. Epps, R.W., Felton, K.C., Coley, C.W., and Abolhasani, M. (2017). Automated microfluidic platform for systematic studies of colloidal perovskite nanocrystals: towards continuous nano-manufacturing. Lab Chip *17*, 4040–4047.

41. Maceiczyk, R.M., Dümbgen, K., Lignos, I., Protesescu, L., Kovalenko, M.V., and deMello, A.J. (2017). Microfluidic reactors provide preparative and mechanistic insights into the synthesis of formamidinium lead halide perovskite nanocrystals. Chem. Mater. *29*, 8433–8439.

42. Lignos, I., Protesescu, L., Emiroglu, D.B., Maceiczyk, R., Schneider, S., Kovalenko, M.V., and deMello, A.J. (2018). Unveiling the shape evolution and halide-ion-segregation in blue-emitting formamidinium lead halide perovskite nanocrystals using an automated microfluidic platform. Nano Lett. *18*, 1246–1252.

43. Liang, X., Baker, R.W., Wu, K., Deng, W., Ferdani, D., Kubiak, P.S., Marken, F., Torrente-Murciano, L., and Cameron, P.J. (2018). Continuous low temperature synthesis of $MAPbX_3$ perovskite nanocrystals in a flow reactor. React. Chem. Eng. *3*, 640–644.

44. Bezinge, L., Maceiczyk, R.M., Lignos, I., Kovalenko, M.V., and deMello, A.J. (2018). Pick a color MARIA: adaptive sampling enables the rapid identification of complex perovskite nanocrystal compositions with defined emission characteristics. ACS Appl. Mater. Interfaces *10*, 18869–18878.

45. Lignos, I., Morad, V., Shynkarenko, Y., Bernasconi, C., Maceiczyk, R.M., Protesescu, L., Bertolotti, F., Kumar, S., Ochsenbein, S.T., and Masciocchi, N. (2018). Exploration of near-infrared-emissive colloidal multinary lead halide perovskite nanocrystals using an automated microfluidic platform. ACS Nano *12*, 5504–5517.

46. Abdel-Latif, K., Epps, R.W., Kerr, C.B., Papa, C.M., Castellano, F.N., and Abolhasani, M. (2019). Facile room-temperature anion exchange reactions of inorganic perovskite quantum dots enabled by a modular microfluidic platform. Adv. Funct. Mater. *29*, 1900712.

47. Kerr, C.B., Epps, R.W., and Abolhasani, M. (2019). A low-cost, non-invasive phase velocity and length meter and controller for multiphase lab-in-a-tube devices. Lab Chip *12*, 2107–2113.

48. Lignos, I., Maceiczyk, R.M., Kovalenko, M.V., and Stavrakis, S. (2019). Tracking the fluorescence lifetimes of cesium lead halide perovskite nanocrystals during their synthesis using a fully automated optofluidic platform. Chem. Mater. *32*, 27–37.

49. Kang, S.-M., Park, B., Raju, G.S.R., Baek, S., Hussain, S.K., Kwak, C.H., Han, Y.-K., Yu, J.S., Kim, S.-W., and Huh, Y.S. (2020). Generation of cesium lead halide perovskite nanocrystals via a serially-integrated microreactor system: sequential anion exchange reaction. Chem. Eng. J. *384*, 123316.

50. Li, S., Baker, R.W., Lignos, I., Yang, Z., Stavrakis, S., Howes, P.D., and deMello, A.J. (2020). Automated microfluidic screening of ligand interactions during the synthesis of cesium lead bromide nanocrystals. Mol. Syst. Des. Eng. https://doi.org/10.1039/D0ME00008F.

51. Epps, R.W., Volk, A.A., Abdel-Latif, K., and Abolhasani, M. (2020). An automated flow chemistry platform to decouple mixing and reaction times. React. Chem. Eng. https://doi.org/10.1039/D0RE00129E.

52. Epps, R.W., Bowen, M.S., Volk, A.A., Abdel-Latif, K., Han, S., Reyes, K.G., Amassian, A., and Abolhasani, M. (2020). Artificial Chemist: an autonomous quantum dot synthesis bot. Adv. Mater. https://doi.org/10.1002/adma.202001626.

53. Zhang, Z., Liu, Y., Geng, C., Shi, S., Zhang, X., Bi, W., and Xu, S. (2019). Rapid synthesis of quantum-confined CsPbBr 3 perovskite nanowires using a microfluidic reactor. Nanoscale *11*, 18790–18796.

54. Elvira, K.S., Solvas, X.C., Wootton, R.C.R., and Demello, A.J. (2013). The past, present and potential for microfluidic reactor technology in chemical synthesis. Nat. Chem. *5*, 905.

55. Jensen, K.F. (2017). Flow chemistry—microreaction technology comes of age. Aiche J. *63*, 858–869.

56. Squires, T.M., and Quake, S.R. (2005). Microfluidics: fluid physics at the nanoliter scale. Rev. Mod. Phys. *77*, 977.

57. Ma, K., Du, X.-Y., Zhang, Y.-W., and Chen, S. (2017). In situ fabrication of halide perovskite nanocrystals embedded in polymer composites via microfluidic spinning microreactors. J. Mater. Chem. C *5*, 9398–9404.

58. Demello, A.J. (2006). Control and detection of chemical reactions in microfluidic systems. Nature *442*, 394–402.

59. Jensen, K.F., Reizman, B.J., and Newman, S.G. (2014). Tools for chemical synthesis in microsystems. Lab Chip *14*, 3206–3212.

60. Abolhasani, M., Coley, C.W., Xie, L., Chen, O., Bawendi, M.G., and Jensen, K.F. (2015). Oscillatory microprocessor for growth and in situ characterization of semiconductor nanocrystals. Chem. Mater. *27*, 6131–6138.

61. Liu, Y., Chen, G., and Yue, J. (2020). Manipulation of gas-liquid-liquid systems in continuous flow microreactors for efficient reaction processes. J. Flow Chem. *10*, 103–121.

62. Huang, H., Polavarapu, L., Sichert, J.A., Susha, A.S., Urban, A.S., and Rogach, A.L. (2016). Colloidal lead halide perovskite nanocrystals: synthesis, optical properties and applications. NPG Asia Mater. *8*, e328.

63. Amgar, D., Aharon, S., and Etgar, L. (2016). Inorganic and hybrid organo-metal perovskite nanostructures: synthesis, properties, and applications. Adv. Funct. Mater. *26*, 8576–8593.

64. Kovalenko, M.V., Protesescu, L., and Bodnarchuk, M.I. (2017). Properties and potential optoelectronic applications of lead halide perovskite nanocrystals. Science *358*, 745–750.

65. Pu, Y., Cai, F., Wang, D., Wang, J.-X., and Chen, J.-F. (2018). Colloidal synthesis of semiconductor quantum dots toward large-scale production: a review. Ind. Eng. Chem. Res. *57*, 1790–1802.

66. Chen, D., and Chen, X. (2019). Luminescent perovskite quantum dots: synthesis, microstructures, optical properties and applications. J. Mater. Chem. C *7*, 1413–1446.

67. Shamsi, J., Urban, A.S., Imran, M., De Trizio, L., and Manna, L. (2019). Metal halide perovskite nanocrystals: synthesis, post-synthesis modifications, and their optical properties. Chem. Rev. *119*, 3296–3348.

68. Lignos, I., Maceiczyk, R., and deMello, A.J. (2017). Microfluidic technology: uncovering the mechanisms of nanocrystal nucleation and growth. Acc. Chem. Res. *50*, 1248–1257.

69. Luo, G., Du, L., Wang, Y., and Wang, K. (2019). Recent developments in microfluidic device-based preparation, functionalization, and manipulation of nano- and micro-materials. Particuology *45*, 1–19.

70. Sui, J., Yan, J., Liu, D., Wang, K., and Luo, G. (2020). Continuous synthesis of nanocrystals via flow chemistry technology. Small *16*, 1902828.

71. Liu, L., Xiang, N., and Ni, Z. (2019). Droplet-based microreactor for the production of micro/nano-materials. Electrophoresis *41*, 833–851.

72. Kubendhiran, S., Bao, Z., Dave, K., and Liu, R.-S. (2019). Microfluidic synthesis of semiconducting colloidal quantum dots and their applications. ACS Appl. Nano Mater. *2*, 1773–1790.

73. Li, S., Hsiao, J.C., Howes, P.D., and deMello, A.J. (2020). Microfluidic tools for the synthesis of bespoke quantum dots. Nanotechnol. Microfluid, 109–148.

74. Nette, J., Howes, P.D., and deMello, A.J. (2020). Microfluidic synthesis of luminescent and plasmonic nanoparticles: fast, efficient, and data-rich. Adv. Mater. Technol. https://doi.org/10.1002/admt.202000060.

75. Vikram, A., Kumar, V., Ramesh, U., Balakrishnan, K., Oh, N., Deshpande, K., Ewers, T., Trefonas, P., Shim, M., and Kenis, P.J.A. (2018). A millifluidic reactor system for multistep continuous synthesis of InP/ZnSeS nanoparticles. ChemNanoMat *4*, 943–953.

76. Kumar, V., Fustér, H.A., Oh, N., Zhai, Y., Deshpande, K., Shim, M., and Kenis, P.J.A. (2017). Continuous flow synthesis of anisotropic cadmium selenide and zinc selenide nanoparticles. ChemNanoMat *3*, 204–211.

77. Baek, J., Shen, Y., Lignos, I., Bawendi, M.G., and Jensen, K.F. (2018). Multistage microfluidic platform for the continuous synthesis of III-V core/shell quantum dots. Angew. Chem. Int. Ed. *57*, 10915–10918.

78. Baek, J., Allen, P.M., Bawendi, M.G., and Jensen, K.F. (2011). Investigation of indium phosphide nanocrystal synthesis using a high-temperature and high-pressure continuous flow microreactor. Angew. Chem. Int. Ed. *50*, 627–630.

79. Guidelli, E.J., Lignos, I., Yoo, J.J., Lusardi, M., Bawendi, M.G., Baffa, O., and Jensen, K.F. (2018). Mechanistic insights and controlled synthesis of radioluminescent ZnSe quantum dots using a microfluidic reactor. Chem. Mater. *30*, 8562–8570.

80. Marre, S., Park, J., Rempel, J., Guan, J., Bawendi, M.G., and Jensen, K.F. (2008). Supercritical continuous-microflow synthesis of narrow size distribution quantum dots. Adv. Mater. *20*, 4830–4834.

81. Nightingale, A.M., and de Mello, J.C. (2009). Controlled synthesis of III-V quantum dots in microfluidic reactors. ChemPhysChem *10*, 2612–2614.

82. Yen, B.K.H., Stott, N.E., Jensen, K.F., and Bawendi, M.G. (2003). A continuous-flow microcapillary reactor for the preparation of a size series of CdSe nanocrystals. Adv. Mater. *15*, 1858–1862.

83. Krishnadasan, S., and Brown, R.J.C. (2007). Intelligent routes to the controlled synthesis of nanoparticles. Lab Chip *7*, 1434–1441.

84. Taylor, G.I. (1953). Dispersion of soluble matter in solvent flowing slowly through a tube. Proc. R. Soc. Lond. Ser. A. Math. Phys. Sci. *219*, 186–203.

85. Nightingale, A.M., Phillips, T.W., Bannock, J.H., and De Mello, J.C. (2014). Controlled multistep synthesis in a three-phase droplet reactor. Nat. Commun. *5*, 3777.

86. Yen, B.K.H., Günther, A., Schmidt, M.A., Jensen, K.F., and Bawendi, M.G. (2005). A microfabricated gas-liquid segmented flow reactor for high-temperature synthesis: the case of CdSe quantum dots. Angew. Chem. Int. Ed. *44*, 5447–5451.

87. Fogler, H.S. (2010). Essentials of Chemical Reaction Engineering (Prentice Hall).

88. Song, H., Bringer, M.R., Tice, J.D., Gerdts, C.J., and Ismagilov, R.F. (2003). Experimental test of scaling of mixing by chaotic advection in droplets moving through microfluidic channels. Appl. Phys. Lett. *83*, 4664–4666.

89. Bringer, M.R., Gerdts, C.J., Song, H., Tice, J.D., and Ismagilov, R.F. (2004). Microfluidic systems for chemical kinetics that rely on chaotic mixing in droplets. Philos. Trans. R. Soc Lond. A. Math. Phys. Eng. Sci. *362*, 1087–1104.

90. Günther, A., Khan, S.A., Thalmann, M., Trachsel, F., and Jensen, K.F. (2004). Transport and reaction in microscale segmented gas-liquid flow. Lab Chip *4*, 278–286.

91. Günther, A., Jhunjhunwala, M., Thalmann, M., Schmidt, M.A., and Jensen, K.F. (2005). Micromixing of miscible liquids in segmented gas-liquid flow. Langmuir *21*, 1547–1555.

92. Shestopalov, I., Tice, J.D., and Ismagilov, R.F. (2004). Multi-step synthesis of nanoparticles performed on millisecond time scale in a microfluidic droplet-based system. Lab Chip *4*, 316–321.

93. Taylor, G.I. (1961). Deposition of a viscous fluid on the wall of a tube. J. Fluid Mech. *10*, 161–165.

94. Kazemi Oskooei, S.A., and Sinton, D. (2010). Partial wetting gas-liquid segmented flow microreactor. Lab Chip *10*, 1732–1734.

95. Baroud, C.N., Gallaire, F., and Dangla, R. (2010). Dynamics of microfluidic droplets. Lab Chip *10*, 2032–2045.

96. Levenspiel, O. (1999). Chemical reaction engineering. Ind. Eng. Chem. Res. *38*, 4140–4143.

97. Kockmann, N. (2007). Transport Phenomena in Micro Process Engineering (Springer Science & Business Media).

98. Stroock, A.D., Dertinger, S.K.W., Ajdari, A., Mezić, I., Stone, H.A., and Whitesides, G.M. (2002). Chaotic mixer for microchannels. Science *295*, 647–651.

99. Ottino, J.M. (1994). Mixing and chemical reactions a tutorial. Chem. Eng. Sci. *49*, 4005–4027.

100. Kreutzer, M.T., Kapteijn, F., Moulijn, J.A., and Heiszwolf, J.J. (2005). Multiphase monolith reactors: chemical reaction engineering of segmented flow in microchannels. Chem. Eng. Sci. *60*, 5895–5916.

101. Karan, D., and Khan, S.A. (2019). Mesoscale triphasic flow reactors for metal catalyzed gas–liquid reactions. React. Chem. Eng. *4*, 1331–1340.

102. Günther, A., and Jensen, K.F. (2006). Multiphase microfluidics: from flow characteristics to chemical and materials synthesis. Lab Chip *6*, 1487–1503.

103. Utada, A.S., Fernandez-Nieves, A., Stone, H.A., and Weitz, D.A. (2007). Dripping to jetting transitions in coflowing liquid streams. Phys. Rev. Lett. *99*, 94502.

104. Li, C., Ding, B., Zhang, L., Song, K., and Tao, S. (2019). 3D-printed continuous flow reactor for high yield synthesis of $CH_3NH_3PbX_3$ (X= Br, I) nanocrystals. J. Mater. Chem. C *7*, 9167–9174.

105. Wei, Z., Chen, Y., Lin, P., Yan, Q., Fan, Y., and Cheng, Z. (2019). Synthesis and encapsulation of all inorganic perovskite nanocrystals by microfluidics. J. Mater. Sci. *54*, 6841–6852.

106. Amjadi, A., Hosseini, M.S., Ashjari, T., Roghabadi, F.A., Ahmadi, V., and Jalili, K. (2020). Durable perovskite UV sensor based on engineered size-tunable polydimethylsiloxane microparticles using a facile capillary microfluidic device from a high-viscosity precursor. ACS Omega *5*, 1052–1061.

107. Lin, W.-Y., Wang, Y., Wang, S., and Tseng, H.-R. (2009). Integrated microfluidic reactors. Nano Today *4*, 470–481.

108. Hartman, R.L., and Jensen, K.F. (2009). Microchemical systems for continuous-flow synthesis. Lab Chip *9*, 2495–2507.

109. de Mello Donegá, C. (2014). Nanoparticles: Workhorses of Nanoscience (Springer).

110. Norris, D.J., and Bawendi, M.G. (1996). Measurement and assignment of the size-dependent optical spectrum in CdSe quantum dots. Phys. Rev. B *53*, 16338.

111. Pietryga, J.M., Park, Y.-S., Lim, J., Fidler, A.F., Bae, W.K., Brovelli, S., and Klimov, V.I. (2016). Spectroscopic and device aspects of nanocrystal quantum dots. Chem. Rev. *116*, 10513–10622.

112. De Roo, J., Ibáñez, M., Geiregat, P., Nedelcu, G., Walravens, W., Maes, J., Martins, J.C., Van Driessche, I., Kovalenko, M.V., and Hens, Z. (2016). Highly dynamic ligand binding and light absorption coefficient of cesium lead bromide perovskite nanocrystals. ACS Nano *10*, 2071–2081.

113. Peter, Y.U., and Cardona, M. (2010). Fundamentals of Semiconductors: Physics and Materials Properties (Springer Science & Business Media).

114. Bodnarchuk, M.I., Boehme, S.C., ten Brinck, S., Bernasconi, C., Shynkarenko, Y., Krieg, F., Widmer, R., Aeschlimann, B., Günther, D., Kovalenko, M.V., et al. (2018). Rationalizing and controlling the surface structure and electronic passivation of cesium lead halide nanocrystals. ACS Energy Lett. *4*, 63–74.

115. Chirvony, V.S., Gonzalez-Carrero, S., Suarez, I., Galian, R.E., Sessolo, M., Bolink, H.J., Martinez-Pastor, J.P., and Perez-Prieto, J. (2017). Luminescence in lead halide perovskite nanocrystals. J. Phys. Chem. C *121*, 13381–13390.

116. Moreels, I., Raino, G., Gomes, R., Hens, Z., Stoferle, T., and Mahrt, R.F. (2011). Band-edge exciton fine structure of small, nearly spherical colloidal CdSe/ZnS quantum dots. ACS Nano *5*, 8033–8039.

117. Pope, M., and Swenberg, C.E. (1999). Electronic Processes in Organic Crystals and Polymers (Oxford University Press on Demand).

118. Park, Y.-S., Guo, S., Makarov, N.S., and Klimov, V.I. (2015). Room temperature single-photon emission from individual perovskite quantum dots. ACS Nano *9*, 10386–10393.

119. Almeida, G., Infante, I., and Manna, L. (2019). Resurfacing halide perovskite nanocrystals. Science *364*, 833–834.

120. Koscher, B.A., Bronstein, N.D., Olshansky, J.H., Bekenstein, Y., and Alivisatos, A.P. (2016). Surface-vs diffusion-limited mechanisms of anion exchange in $CsPbBr_3$ nanocrystal cubes revealed through kinetic studies. J. Am. Chem. Soc. *138*, 12065–12068.

121. Li, X., Ji, M., Li, H., Wang, H., Xu, M., Rong, H., Wei, J., Liu, J., Liu, J., and Chen, W. (2020). Cation/anion exchange reactions toward the syntheses of upgraded nanostructures: principles and applications. Matter *2*, 554–586.

122. Bekenstein, Y., Koscher, B.A., Eaton, S.W., Yang, P., and Alivisatos, A.P. (2015). Highly luminescent colloidal nanoplates of perovskite cesium lead halide and their oriented assemblies. J. Am. Chem. Soc. *137*, 16008–16011.

123. Riedinger, A., Ott, F.D., Mule, A., Mazzotti, S., Knüsel, P.N., Kress, S.J.P., Prins, F., Erwin, S.C., and Norris, D.J. (2017). An intrinsic growth instability in isotropic materials leads to quasi-two-dimensional nanoplatelets. Nat. Mater. *16*, 743–748.

124. Almeida, G., Goldoni, L., Akkerman, Q., Dang, Z., Khan, A.H., Marras, S., Moreels, I., and Manna, L. (2018). Role of acid-base equilibria in the size, shape, and phase control of cesium lead bromide nanocrystals. ACS Nano *12*, 1704–1711.

125. Pan, A., He, B., Fan, X., Liu, Z., Urban, J.J., Alivisatos, A.P., He, L., and Liu, Y. (2016). Insight into the ligand-mediated synthesis of colloidal $CsPbBr_3$ perovskite nanocrystals: the role of organic acid, base, and cesium precursors. ACS Nano *10*, 7943–7954.

126. Nenon, D.P., Pressler, K., Kang, J., Koscher, B.A., Olshansky, J.H., Osowiecki, W.T., Koc, M.A., Wang, L.-W., and Alivisatos, A.P. (2018). Design principles for trap-free $CsPbX_3$ nanocrystals: enumerating and eliminating surface halide vacancies with softer lewis bases. J. Am. Chem. Soc. *140*, 17760–17772.

127. Weidman, M.C., Seitz, M., Stranks, S.D., and Tisdale, W.A. (2016). Highly tunable colloidal perovskite nanoplatelets through variable cation, metal, and halide composition. ACS Nano *10*, 7830–7839.

128. Murray, C.b., Norris, D.J., and Bawendi, M.G. (1993). Synthesis and characterization of nearly monodisperse CdE (E= sulfur, selenium, tellurium) semiconductor nanocrystallites. J. Am. Chem. Soc. *115*, 8706–8715.

129. Murray, C.B., Kagan, A.C.R., and Bawendi, M.G. (2000). Synthesis and characterization of monodisperse nanocrystals and close-packed nanocrystal assemblies. Annu. Rev. Mater. Sci. *30*, 545–610.

130. Pan, J., El-Ballouli, A.O., Rollny, L., Voznyy, O., Burlakov, V.M., Goriely, A., Sargent, E.H., and Bakr, O.M. (2013). Automated synthesis of photovoltaic-quality colloidal quantum dots using separate nucleation and growth stages. ACS Nano *7*, 10158–10166.

131. Chiba, T., Hayashi, Y., Ebe, H., Hoshi, K., Sato, J., Sato, S., Pu, Y.-J., Ohisa, S., and Kido, J. (2018). Anion-exchange red perovskite quantum dots with ammonium iodine salts for highly efficient light-emitting devices. Nat. Photon. *12*, 681–687.

132. Gong, X., Yang, Z., Walters, G., Comin, R., Ning, Z., Beauregard, E., Adinolfi, V., Voznyy, O., and Sargent, E.H. (2016). Highly efficient quantum dot near-infrared light-emitting diodes. Nat. Photon. *10*, 253–257.

133. Vasilopoulou, M., Kim, H.P., Kim, B.S., Papadakis, M., Ximim Gavim, A.E., Macedo, A.G., Jose da Silva, W., Schneider, F.K., Mat Teridi, M.A., Coutsolelos, A.G., et al. (2020). Efficient colloidal quantum dot light-emitting diodes operating in the second near-infrared biological window. Nat. Photon. *14*, 50–56.

134. Mali, S.S., Shim, C.S., and Hong, C.K. (2015). Highly stable and efficient solid-state solar cells based on methylammonium lead bromide ($CH_3NH_3PbBr_3$) perovskite quantum dots. NPG Asia Mater. *7*, e208.

135. García de Arquer, F.P., Armin, A., Meredith, P., and Sargent, E.H. (2017). Solution-processed semiconductors for next-generation photodetectors. Nat. Rev. Mater. *2*, 16100.

136. Zhu, X., Bian, L., Fu, H., Wang, L., Zou, B., Dai, Q., Zhang, J., and Zhong, H. (2020). Broadband perovskite quantum dot spectrometer beyond human visual resolution. Light Sci. Appl. *9*, 73.

137. Rhee, J.H., Chung, C.-C., and Diau, E.W.-G. (2013). A perspective of mesoscopic solar cells based on metal chalcogenide quantum dots and organometal-halide perovskites. NPG Asia Mater. *5*, e68.

138. Nayak, P.K., Mahesh, S., Snaith, H.J., and Cahen, D. (2019). Photovoltaic solar cell technologies: analysing the state of the art. Nat. Rev. Mater. *4*, 269–285.

139. Semonin, O.E., Luther, J.M., and Beard, M.C. (2012). Quantum dots for next-generation photovoltaics. Mater. Today *15*, 508–515.

140. Nozik, A.J., Beard, M.C., Luther, J.M., Law, M., Ellingson, R.J., and Johnson, J.C. (2010). Semiconductor quantum dots and quantum dot arrays and applications of multiple exciton generation to third-generation photovoltaic solar cells. Chem. Rev. *110*, 6873–6890.

141. Jensen, K.F., Coley, C.W., and Eyke, N.S. (2019). Autonomous discovery in the chemical sciences part I: progress. Angew. Chem. Int. Ed. https://doi.org/10.1002/anie.201909987.

142. Coley, C.W., Eyke, N.S., and Jensen, K.F. (2019). Autonomous discovery in the chemical sciences part II: outlook. Angew. Chem. Int. Ed. https://doi.org/10.1002/anie.201909989.

143. Silver, D., Hubert, T., Schrittwieser, J., Antonoglou, I., Lai, M., Guez, A., Lanctot, M., Sifre, L., Kumaran, D., Graepel, T., et al. (2018). A general reinforcement learning algorithm that masters chess, shogi, and Go through self-play. Science *362*, 1140 LP–1144.

144. Dimitrov, T., Kreisbeck, C., Becker, J.S., Aspuru-Guzik, A., and Saikin, S.K. (2019). Autonomous molecular design: then and now. ACS Appl. Mater. Inter. *11*, 24825–24836.

145. Correa-Baena, J.-P., Hippalgaonkar, K., van Duren, J., Jaffer, S., Chandrasekhar, V.R., Stevanovic, V., Wadia, C., Guha, S., and Buonassisi, T. (2018). Accelerating materials development via automation, machine learning, and high-performance computing. Joule *2*, 1410–1420.

146. Cronin, L., Porwol, L., Kowalski, D., Henson, A., Long, D.-L., and Bell, N. (2020). An autonomous chemical robot discovers the rules of supramolecular chemistry without prior knowledge. Angew. Chem. Int. Ed. https://doi.org/10.1002/anie.202000329.

147. Kirman, J., Johnston, A., Kuntz, D.A., Askerka, M., Gao, Y., Todorović, P., Ma, D., Privé, G.G., and Sargent, E.H. (2020). Machine-learning-accelerated perovskite crystallization. Matter. https://doi.org/10.1016/j.matt.2020.02.012.

148. Barnard, A.S., Motevalli, B., Parker, A.J., Fischer, J.M., Feigl, C.A., and Opletal, G. (2019). Nanoinformatics, and the big challenges for the science of small things. Nanoscale *11*, 19190–19201.

149. Abolhasani, M., Singh, M., Kumacheva, E., and Günther, A. (2012). Cruise control for segmented flow. Lab Chip *12*, 4787–4795.

150. Harvie, A.J., and deMello, J.C. (2020). Optical determination of flow-rate and flow-uniformity in segmented flows. Chem. Eng. J. *394*, 124908.

151. Hou, S., Gangishetty, M.K., Quan, Q., and Congreve, D.N. (2018). Efficient blue and white perovskite light-emitting diodes via manganese doping. Joule *2*, 2421–2433.

152. Guria, A.K., Dutta, S.K., Das Adhikari, S., and Pradhan, N. (2017). Doping Mn^{2+} in lead halide perovskite nanocrystals: successes and challenges. ACS Energy Lett. *2*, 1014–1021.

153. Boles, M.A., Ling, D., Hyeon, T., and Talapin, D.V. (2016). The surface science of nanocrystals. Nat. Mater. *15*, 141.

154. Yin, Y., and Alivisatos, A.P. (2005). Colloidal nanocrystal synthesis and the organic-inorganic interface. Nature *437*, 664–670.

155. Lu, H., Zhu, X., Miller, C., San Martin, J., Chen, X., Miller, E.M., Yan, Y., and Beard, M.C. (2019). Enhanced photoredox activity of $CsPbBr_3$ nanocrystals by quantitative colloidal ligand exchange. J. Chem. Phys. *151*, 204305.

156. Pan, J., Sarmah, S.P., Murali, B., Dursun, I., Peng, W., Parida, M.R., Liu, J., Sinatra, L., Alyami, N., and Zhao, C. (2015). Air-stable surface-passivated perovskite quantum dots for ultra-robust, single- and two-photon-induced amplified spontaneous emission. J. Phys. Chem. Lett. *6*, 5027–5033.

157. Luther, J.M., Law, M., Song, Q., Perkins, C.L., Beard, M.C., and Nozik, A.J. (2008). Structural, optical, and electrical properties of self-assembled films of PbSe nanocrystals treated with 1,2-ethanedithiol. ACS Nano *2*, 271–280.

158. Zhou, H., Chen, Q., Li, G., Luo, S., Song, T., Duan, H.-S., Hong, Z., You, J., Liu, Y., and Yang, Y. (2014). Interface engineering of highly efficient perovskite solar cells. Science *345*, 542–546.

159. Im, J.-H., Lee, C.-R., Lee, J.-W., Park, S.-W., and Park, N.-G. (2011). 6.5% efficient perovskite quantum-dot-sensitized solar cell. Nanoscale *3*, 4088–4093.

160. Rainò, G., Becker, M.A., Bodnarchuk, M.I., Mahrt, R.F., Kovalenko, M.V., and Stöferle, T. (2018). Superfluorescence from lead halide perovskite quantum dot superlattices. Nature *563*, 671–675.

161. Kirmani, A.R., Carey, G.H., Abdelsamie, M., Yan, B., Cha, D., Rollny, L.R., Cui, X., Sargent, E.H., and Amassian, A. (2014). Effect of solvent environment on colloidal-quantum-dot solar-cell manufacturability and performance. Adv. Mater. *26*, 4717–4723.

162. Kirmani, A.R., Walters, G.W., Kim, T., Sargent, E.H., and Amassian, A. (2020). Optimizing solid-state ligand exchange for colloidal quantum dot optoelectronics: how much is enough? ACS Appl. Energy Mater. https://doi.org/10.1021/acsaem.0c00389.

163. Fischer, A., Rollny, L., Pan, J., Carey, G.H., Thon, S.M., Hoogland, S., Voznyy, O., Zhitomirsky, D., Kim, J.Y., and Bakr, O.M. (2013). Directly deposited quantum dot solids using a colloidally stable nanoparticle ink. Adv. Mater. *25*, 5742–5749.

164. Kroupa, D.M., Vörös, M., Brawand, N.P., McNichols, B.W., Miller, E.M., Gu, J., Nozik, A.J., Sellinger, A., Galli, G., and Beard, M.C. (2017). Tuning colloidal quantum dot band edge positions through solution-phase surface chemistry modification. Nat. Commun. *8*, https://doi.org/10.1038/ncomms15257.

165. Sun, S. (2019). Accelerated development of perovskite-inspired materials via high-throughput synthesis and machine-learning diagnosis. Joule *3*, 1437–1451.

166. Lakowicz, J.R. (2006). Principles of Fluorescence Spectroscopy (Springer).

167. Mäntele, W., and Deniz, E. (2017). UV-VIS absorption spectroscopy: Lambert-Beer reloaded. Spectrochim. Acta A Mol. Biomol. Spectrosc. *173*, 965–968.

168. Kubista, M., Sjöback, R., Eriksson, S., and Albinsson, B. (1994). Experimental correction for the inner-filter effect in fluorescence spectra. Analyst *119*, 417–419.

169. de Weerd, C., Gomez, L., Zhang, H., Buma, W.J., Nedelcu, G., Kovalenko, M.V., and Gregorkiewicz, T. (2016). Energy transfer between inorganic perovskite nanocrystals. J. Phys. Chem. C *120*, 13310–13315.

170. Zhang, T., Li, G., Chang, Y., Wang, X., Zhang, B., Mou, H., and Jiang, Y. (2017). Full-spectra

hyperfluorescence cesium lead halide perovskite nanocrystals obtained by efficient halogen anion exchange using zinc halogenide salts. Cryst. Eng. Commun. *19*, 1165–1171.

171. Zhou, Y., Zhou, H., Deng, J., Cha, W., and Cai, Z. (2020). Decisive structural and functional characterization of halide perovskites with synchrotron. Matter *2*, 360–377.

172. Yue, J., Schouten, J.C., and Nijhuis, T.A. (2012). Integration of microreactors with spectroscopic detection for online reaction monitoring and catalyst characterization. Ind. Eng. Chem. Res. *51*, 14583–14609.

173. Marmiroli, B., Grenci, G., Cacho-Nerin, F., Sartori, B., Ferrari, E., Laggner, P., Businaro, L., and Amenitsch, H. (2009). Free jet micromixer to study fast chemical reactions by small angle X-ray scattering. Lab Chip *9*, 2063–2069.

174. Polte, J., Erler, R., Thunemann, A.F., Sokolov, S., Ahner, T.T., Rademann, K., Emmerling, F., and Kraehnert, R. (2010). Nucleation and growth of gold nanoparticles studied via in situ small angle X-ray scattering at millisecond time resolution. ACS Nano *4*, 1076–1082.

175. Oyanagi, H., Sun, Z.H., Jiang, Y., Uehara, M., Nakamura, H., Yamashita, K., Zhang, L., Lee, C., Fukano, A., and Maeda, H. (2011). In situ XAFS experiments using a microfluidic cell: application to initial growth of CdSe nanocrystals. J. Synchrotron Radiat. *18*, 272–279.

176. Sun, Z.H., Oyanagi, H., Uehara, M., Nakamura, H., Yamashita, K., Fukano, A., and Maeda, H. (2009). Study on initial kinetics of CdSe nanocrystals by a combination of in situ X-ray absorption fine structure and microfluidic reactor. J. Phys. Chem. C *113*, 18608–18613.

177. Maceiczyk, R.M., Lignos, I.G., and deMello Andrew, J. (2015). Online detection and automation methods in microfluidic nanomaterial synthesis. Curr. Opin. Chem. Eng. *8*, 29–35.

178. Chan, E.M., Marcus, M.A., Fakra, S., El Naggar, M., Mathies, R.A., and Alivisatos, A.P. (2007). Millisecond kinetics of nanocrystal cation exchange using microfluidic X-ray absorption spectroscopy. J. Phys. Chem. A *111*, 12210–12215.

179. Ravi, V.K., Santra, P.K., Joshi, N., Chugh, J., Singh, S.K., Rensmo, H., Ghosh, P., and Nag, A. (2017). Origin of the substitution mechanism for the binding of organic ligands on the surface of $CsPbBr_3$ perovskite nanocubes. J. Phys. Chem. Lett. *8*, 4988–4994.

180. Lacey, M.E., Subramanian, R., Olson, D.L., Webb, A.G., and Sweedler, J.V. (1999). High-resolution NMR spectroscopy of sample volumes from 1 nL to 10 μL. Chem. Rev. *99*, 3133–3152.

181. Van Bentum, P.J.M., Janssen, J.W.G., and Kentgens, A.P.M. (2004). Towards nuclear magnetic resonance μ-spectroscopy and μ-imaging. Analyst *129*, 793–803.

182. Bart, J., Kolkman, A.J., Oosthoek-de Vries, A.J., Koch, K., Nieuwland, P.J., Janssen, H., van Bentum, J., Ampt, K.A.M., Rutjes, F.P.J.T., and Wijmenga, S.S. (2009). A microfluidic high-resolution NMR flow probe. J. Am. Chem. Soc. *131*, 5014–5015.

183. Gomez, M.V., Verputten, H.H.J., Díaz-Ortíz, A., Moreno, A., de la Hoz, A., and Velders, A.H. (2010). On-line monitoring of a microwave-assisted chemical reaction by nanolitre NMR-spectroscopy. Chem. Commun. *46*, 4514–4516.

184. Sans, V., and Cronin, L. (2016). Towards dial-a-molecule by integrating continuous flow, analytics and self-optimisation. Chem. Soc. Rev. *45*, 2032–2043.

185. Takahashi, Y., Nakakoshi, M., Sakurai, S., Akiyama, Y., Suematsu, H., Utsumi, H., and Kitamori, T. (2007). Development of an NMR interface microchip "MICCS" for direct detection of reaction products and intermediates of micro-syntheses using a "MICCS-NMR". Anal. Sci. *23*, 395–400.

186. Mompeán, M., Sánchez-Donoso, R.M., De La Hoz, A., Saggiomo, V., Velders, A.H., and Gomez, M.V. (2018). Pushing nuclear magnetic resonance sensitivity limits with microfluidics and photo-chemically induced dynamic nuclear polarization. Nat. Commun. *9*, https://doi.org/10.1038/s41467-017-02575-0.

187. Carabatos-Nédelec, C., Oussaïd, M., and Nitsch, K. (2003). Raman scattering investigation of cesium plumbochloride, $CsPbCl_3$, phase transitions. J. Raman Spectrosc. *34*, 388–393.

188. Guo, Y., Yaffe, O., Paley, D.W., Beecher, A.N., Hull, T.D., Szpak, G., Owen, J.S., Brus, L.E., and Pimenta, M.A. (2017). Interplay between organic cations and inorganic framework and incommensurability in hybrid lead-halide perovskite $CH_3NH_3PbBr_3$. Phys. Rev. Mater. *1*, 42401.

189. Niemann, R.G., Kontos, A.G., Palles, D., Kamitsos, E.I., Kaltzoglou, A., Brivio, F., Falaras, P., and Cameron, P.J. (2016). Halogen effects on ordering and bonding of $CH_3NH_3^+$ in $CH_3NH_3PbX_3$ (X= Cl, Br, I) hybrid perovskites: a vibrational spectroscopic study. J. Phys. Chem. C *120*, 2509–2519.

190. Zhao, F., Cambie, D., Janse, J., Wieland, E.W., Kuijpers, K.P.L., Hessel, V., Debije, M.G., and Noël, T. (2018). Scale-up of a luminescent solar concentrator-based photomicroreactor via numbering-up. ACS Sustain. Chem. Eng. *6*, 422–429.

191. Liao, M., Shan, B., and Li, M. (2019). In situ Raman spectroscopic studies of thermal stability of all-inorganic cesium lead halide ($CsPbX_3$, X= Cl, Br, I) perovskite nanocrystals. J. Phys. Chem. Lett. *10*, 1217–1225.

192. Jahn, I.J., Žukovskaja, O., Zheng, X.-S., Weber, K., Bocklitz, T.W., Cialla-May, D., and Popp, J. (2017). Surface-enhanced Raman spectroscopy and microfluidic platforms: challenges, solutions and potential applications. Analyst *142*, 1022–1047.

193. März, A., Henkel, T., Cialla, D., Schmitt, M., and Popp, J. (2011). Droplet formation via flow-through microdevices in Raman and surface enhanced Raman spectroscopy—concepts and applications. Lab Chip *11*, 3584–3592.

194. Yazdi, S.H., Giles, K.L., and White, I.M. (2013). Multiplexed detection of DNA sequences using a competitive displacement assay in a microfluidic SERRS-based device. Anal. Chem. *85*, 10605–10611.

195. Smith, E., and Dent, G. (2019). Modern Raman Spectroscopy: A Practical Approach (John Wiley & Sons).

196. Mendorf, M., Nachtrodt, H., Mescher, A., Ghaini, A., and Agar, D.W. (2010). Design and control techniques for the numbering-up of capillary microreactors with uniform multiphase flow distribution. Ind. Eng. Chem. Res. *49*, 10908–10916.

197. Nightingale, A.M., Bannock, J.H., Krishnadasan, S.H., O'Mahony, F.T.F., Haque, S.A., Sloan, J., Drury, C., McIntyre, R., and deMello, J.C. (2013). Large-scale synthesis of nanocrystals in a multichannel droplet reactor. J. Mater. Chem. A *1*, 4067–4076.

198. Zhang, J., Wang, K., Teixeira, A.R., Jensen, K.F., and Luo, G. (2017). Design and scaling up of microchemical systems: a review. Annu. Rev. Chem. Biomol. Eng. *8*, 285–305.

199. Ahn, G.-N., Yu, T., Lee, H.-J., Gyak, K.-W., Kang, J.-H., You, D., and Kim, D.-P. (2019). A numbering-up metal microreactor for the high-throughput production of a commercial drug by copper catalysis. Lab Chip *19*, 3535–3542.

200. Riche, C.T., Roberts, E.J., Gupta, M., Brutchey, R.L., and Malmstadt, N. (2016). Flow invariant droplet formation for stable parallel microreactors. Nat. Commun. *7*, https://doi.org/10.1038/ncomms10780.

201. Wang, L., Karadaghi, L.R., Brutchey, R.L., and Malmstadt, N. (2020). Self-optimizing parallel millifluidic reactor for scaling nanoparticle synthesis. Chem. Commun. *56*, 3745–3748.

202. Bannock, J.H., Lui, T.Y.M., Turner, S.T., and deMello, J.C. (2018). Automated separation of immiscible liquids using an optically monitored porous capillary. React. Chem. Eng. *3*, 467–477.

203. Niu, G., Zhang, L., Ruditskiy, A., Wang, L., and Xia, Y. (2018). A droplet-reactor system capable of automation for the continuous and scalable production of noble-metal nanocrystals. Nano Lett. *18*, 3879–3884.

204. Shen, Y., Gee, M.Y., and Greytak, A.B. (2017). Purification technologies for colloidal nanocrystals. Chem. Commun. *53*, 827–841.

205. Shen, Y., Weeranoppanant, N., Xie, L., Chen, Y., Lusardi, M.R., Imbrogno, J., Bawendi, M.G., and Jensen, K.F. (2017). Multistage extraction platform for highly efficient and fully continuous purification of nanoparticles. Nanoscale *9*, 7703–7707.

206. Shen, Y., Abolhasani, M., Chen, Y., Xie, L., Yang, L., Coley, C.W., Bawendi, M.G., and Jensen, K.F. (2017). In-situ microfluidic study of biphasic nanocrystal ligand-exchange reactions using an oscillatory flow reactor. Angew. Chem. Int. Ed. *56*, 16333–16337.